



Effect of dolomitization on isotopic records from Neoproterozoic carbonates in southwestern Mongolia

Uyanga Bold^{a,b,*}, Anne-Sofie Crüger Ahm^c, Daniel P. Schrag^d, John A. Higgins^c, Erdenebayar Jamsran^e, Francis A. Macdonald^f

^a Department of Research and Cooperation, Mongolian University of Science and Technology, 8th khoroo, Baga toiruu 34, Sukhaaatar District, Ulaanbaatar 14191, Mongolia

^b Earth Science Center of Mongolia, National Information Technology Park, Baga Toiruu-20, Ulaanbaatar 14200, Mongolia

^c Department of Geosciences, Princeton University, Guyot Hall, Washington Road, Princeton, NJ 08544, United States

^d Earth and Planetary Sciences Department, Harvard University, Cambridge, MA 02138, United States

^e School of Geology and Mining Engineering, Mongolian University of Science and Technology, 8th khoroo, Baga toiruu 34, Sukhaaatar District, Ulaanbaatar 14191, Mongolia

^f Department of Earth Science, University of California, Santa Barbara, CA 93106, United States

ARTICLE INFO

Keywords:

Chemostratigraphy
Neoproterozoic
Dolomitization
Isotopic variability
Fluid inclusion

ABSTRACT

Carbon isotope values from shallow-marine carbonate rocks, including those from many dolomitized successions, are the primary lens through which we interpret the ancient carbon cycle. Carbon isotopes are typically regarded as being robust to alteration during dolomitization due to the high carbon content of the rock compared to the fluid. However, chemostratigraphic studies of the Neoproterozoic Tsagaan-Olom Group in southwestern Mongolia exhibit 3–12‰ differences in carbon isotopes between stratigraphically equivalent limestone and dolomitized successions. To understand the origins of this geochemical variation, we conducted detailed geological mapping, petrographic, isotopic ($\delta^{13}\text{C}$, $\delta^{18}\text{O}$, $\delta^{44/40}\text{Ca}$, and $\delta^{26}\text{Mg}$), and fluid inclusion analyses of carbonates in the Taishir, Ol, and Shuurgat formations of the Tsagaan-Olom Group. Stratigraphic and textural constraints distinguish fabric retentive early dolomitization (Dolomitization Event 1) that occurred in the Taishir and Ol formations during and soon after deposition of the ca. 635 Ma Marinoan cap dolomite of the Ol Formation and fabric destructive dolomitization that occurred after the deposition of the younger Shuurgat Formation (Dolomitization Event 2), either prior to or during early Cambrian foreland basin formation. The dolomitizing fluids moved through porous stratigraphic units bound by impermeable shale of the Khongor and Zuun-Arts formations. Dolomitization homogenized the isotopic records of all Neoproterozoic Tsagaan-Olom Group dolomites; undolomitized successions show more extreme negative excursions from more positive background values. The salinity and isotopic values of seawater, the dolomitizing fluids, and the original platform carbonate were estimated from fluid inclusion data and a numerical model of diagenetic dolomitization. These results demonstrate that both early and late dolomitization can have a profound effect on carbon isotopic records of carbonates; however, with a multi-isotope approach the original carbon isotopic composition of platform-top carbonate can be distinguished from that of seawater and other dolomitizing fluids.

1. Introduction

Proterozoic and Paleozoic platform carbonates are dominated by dolostone (e.g., Arvidson and Mackenzie, 1999; Morrow, 1982; Warren, 2000). Isotopic records from these dolostone successions, and particularly Proterozoic dolomites, are commonly used to reconstruct the chemistry of ancient oceans (e.g., Brand, 2004; Halverson et al., 2010; Kaufman and Knoll, 1995; Melchin and Holmden, 2006). Although some studies suggest that the abundance of dolomite in Proterozoic and

Archean carbonates can be attributed to environmental changes (e.g., temperature and seawater chemistry) that resulted in increased precipitation of primary dolomite from seawater (e.g., Arvidson and Mackenzie, 1999), it is generally agreed that the majority of ancient dolomite is a replacement product.

Carbon isotope records in dolomite successions have played an important role in the interpretation of Neoproterozoic environmental change. Because dolomitizing fluids have abundant oxygen and relatively little carbon (Land, 1985), oxygen isotopes ($\delta^{18}\text{O}$) in dolomite are

* Corresponding author.

commonly interpreted to reflect the composition and temperature of dolomitizing fluids whereas carbon isotopes ($\delta^{13}\text{C}$) are thought to be rock-buffered and reflect the isotopic composition of the precursor carbonate (Degens and Epstein, 1964). Consequently, $\delta^{13}\text{C}$ values from ancient dolomites are widely used as archives of the global carbon cycle in Earth history. Impressive stratigraphic reproducibility of $\delta^{13}\text{C}$ values and detailed textural studies in dolomites from Namibia (Halverson et al., 2002; Kaufman et al., 1991) and Svalbard (Halverson et al., 2004) support the common assumption that $\delta^{13}\text{C}$ values are rock-buffered and preserve the carbon isotopic composition of the precursor carbonate minerals. Together with other geologic and geochemical evidence ($^{87}\text{Sr}/^{86}\text{Sr}$, biostratigraphy, etc.), $\delta^{13}\text{C}$ values have also been used to correlate Paleozoic carbonate strata worldwide (Saltzman and Sedlacek, 2013). These records have been used to construct Neoproterozoic and Paleozoic composite $\delta^{13}\text{C}$ curves, which are characterized by extended periods of positive $\delta^{13}\text{C}$ values and brief intervals with negative $\delta^{13}\text{C}$ excursions (e.g., Halverson, 2006; Rose et al., 2012; Saltzman and Thomas, 2012).

Although carbon isotope chemostratigraphy is an invaluable tool in the Proterozoic, it is not without its problems. Broadly correlative Cryogenian carbonate-dominated successions in Namibia, Arctic Alaska, and Mongolia (Macdonald et al., 2009a, 2009b) preserve significant differences in the absolute $\delta^{13}\text{C}$ values that are difficult to explain with diachroneity. Particularly, background $\delta^{13}\text{C}$ values from limestone in Mongolia are more enriched in ^{13}C (Fig. 1) than coincident records of dolomitized strata from Namibia and Arctic Alaska (Macdonald et al., 2009a,b).

Along with differences in $\delta^{13}\text{C}$ profiles between stratigraphically equivalent successions on different Proterozoic margins, spatial

gradients in $\delta^{13}\text{C}$ values have also been observed on individual margins. Variable $\delta^{13}\text{C}$ values have been measured between dolomitized Ediacaran carbonates deposited in platform and fore-slope settings in Namibia (Ahm et al., 2019; Hoffman, 2011) and platform, slope, and basin settings in South China (Jiang et al., 2007). In general, this spatial variability in $\delta^{13}\text{C}$ values has been attributed to surface-to-deep ocean $\delta^{13}\text{C}$ gradients derived from the cycling (production and respiration) of organic carbon or differences in the $\delta^{13}\text{C}$ of dissolved inorganic carbonate (DIC) due to differences in temperature or ocean circulation (Grotzinger and Knoll, 1995; Hoffman, 2011). However, prior to the Jurassic, deep sea drill cores are unavailable, and sediments preserved on continental margins or carbonate banks are variably affected by platform processes such as early dolomitization, and are not necessarily passive records of ocean DIC (Higgins et al., 2018).

Calcium and Mg isotopes ($\delta^{44/40}\text{Ca}$ and $\delta^{26}\text{Mg}$) can provide insights into carbonate diagenesis and dolomitization because Ca and Mg are major components of carbonates and diagenetic resetting therefore requires extensive fluid advection/diffusion (Ahm et al., 2018; Fantle and Higgins, 2014; Higgins et al., 2018). As a result, the pairing of $\delta^{44/40}\text{Ca}$ and $\delta^{26}\text{Mg}$ values provides a tool to identify the style and extent of early diagenetic alteration and dolomitization of carbonate sediments. Dolomitization can result in covariation between $\delta^{44/40}\text{Ca}$ and $\delta^{26}\text{Mg}$ for three reasons. First, early diagenetic dolomites are characterized by a small Ca isotope fractionation factor compared to primary marine carbonate minerals (Fantle and DePaolo, 2007; Gussone et al., 2020, 2005; Jacobson and Holmden, 2008). Second, dolomitization can occur under both fluid- and sediment-buffered conditions, depending on the extent to which pore-fluid exchange with seawater occurs through advection or diffusion. Third, Mg incorporation into diagenetic dolomites

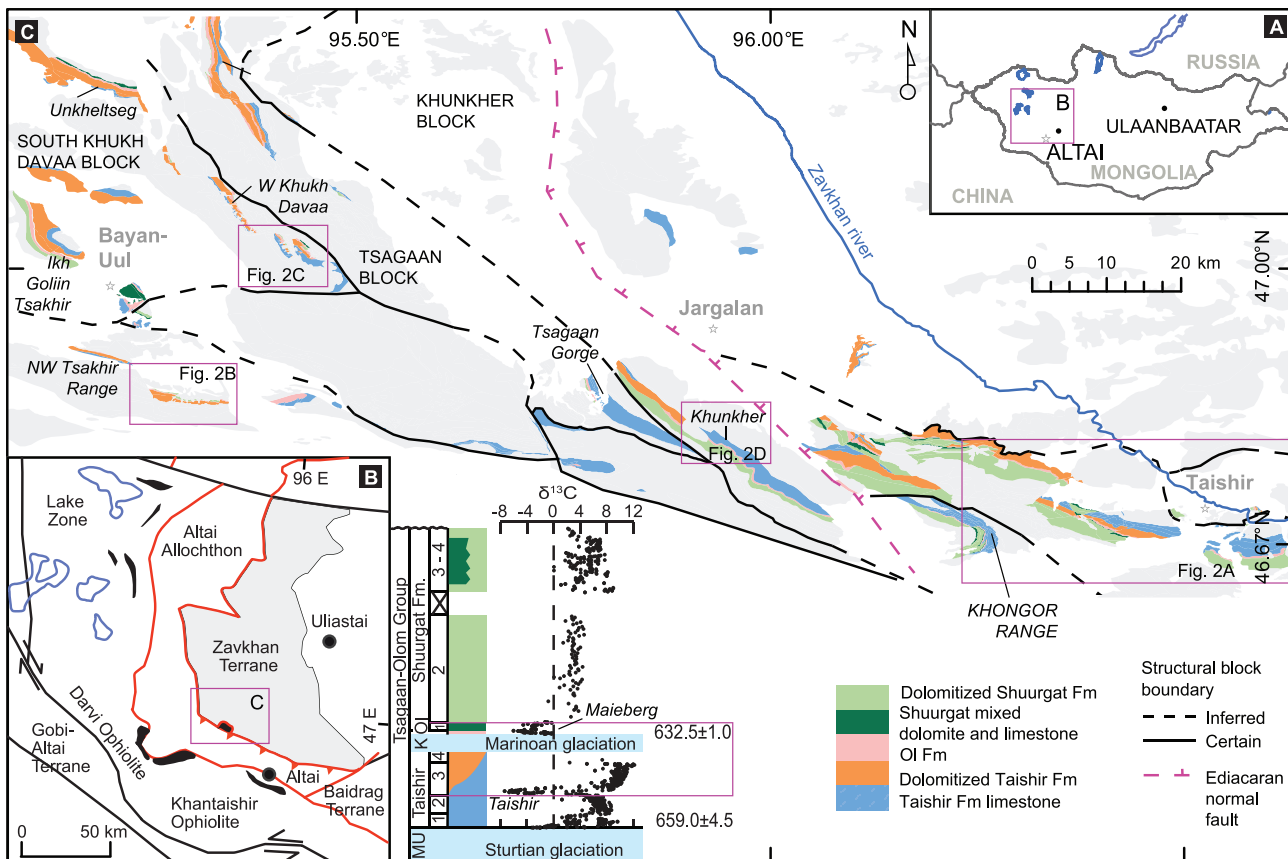


Fig. 1. Outline map of the Zavkhan Terrane showing the extent of dolomitized carbonates of the Tsagaan-Olom Group. A) Location map of the study area. B) Simplified terrane map of southwestern Mongolia. Extent of inset map C is boxed. C) Simplified geological map of the Zavkhan Terrane. Dolomitized carbonates of the Taishir, Ol, and Shuurgat formations are shown. Extent of Fig. 2A-D are highlighted by boxes as well as the carbonate successions affected by the main dolomitization event (members 3 and 4 of the Taishir and Ol formations). The plot of $\delta^{13}\text{C}$ values is from Bold et al. (2016b).

is associated with a -2\textpercent isotopic fractionation factor (Higgins and Schrag, 2010), leading to Rayleigh-type distillation of the pore-fluid in closed-system settings (Blättler et al., 2015). As a result, dolomites that form under fluid-buffered conditions have lower $\delta^{26}\text{Mg}$ and higher $\delta^{44}/\delta^{40}\text{Ca}$ values than dolomites that form in a sediment-buffered conditions. Together, these isotopic properties lead to characteristic relationships between bulk $\delta^{44}/\delta^{40}\text{Ca}$ and $\delta^{26}\text{Mg}$ values and provide a means to disentangle the extend of early marine fluid-buffered versus sediment-buffered dolomitization. This framework has previously provided insights into the origins of the “Shuram” negative $\delta^{13}\text{C}$ excursion (Husson et al., 2015), Bahama Banks dolomites (Higgins et al., 2018), basal Ediacaran “cap dolostones” (Ahm et al., 2019), and Hirnantian carbonates (Jones et al., 2020). In these studies, rather than interpreting each of the elemental and isotopic systems ($\delta^{44}/\delta^{40}\text{Ca}$, $\delta^{26}\text{Mg}$, $\delta^{18}\text{O}$ and $\delta^{13}\text{C}$) on their own, the systematic correlation and covariation among these systems have been integrated to understand the diagenetic history. Here we apply this approach to dolomites of the Neoproterozoic Tsagaan-Olom Group in Mongolia to better constrain the origin and diagenetic history of these dolomites.

The Neoproterozoic Tsagaan-Olom Group of Mongolia is composed of stratigraphically equivalent limestone and dolomitized strata that provide an excellent opportunity to document the geochemical consequences of dolomitization (Fig. 1). Limestone sections of the Tsagaan-Olom Group covary in $\delta^{13}\text{C}_{\text{carb}}$ and $\delta^{13}\text{C}_{\text{org}}$ values (Johnston et al., 2012), which suggests that measured $\delta^{13}\text{C}$ values record the original isotopic composition of DIC in the surface waters of the carbonate ramp (but not necessarily the whole ocean). In contrast, the $\delta^{13}\text{C}$ values of the dolomitized equivalent strata of the Taishir, Ol, and Shuurgat formations (fms) record significant variability (Bold et al., 2016b). By including new Ca and Mg measurements, we document differences in geochemical proxies preserved in stratigraphically equivalent limestone and dolostone successions in the Tsagaan-Olom Group, develop a model for their dolomitization, and discuss how these results inform the interpretation of geochemical records obtained from other ancient carbonate successions.

2. Geological setting

The Zavkhan Terrane of southwestern Mongolia is a Neoproterozoic ribbon continent that was incorporated into the Central Asian orogenic belt (e.g., Windley et al., 2007). The basement gneiss of the Zavkhan Terrane is ca. 1967 Ma and is intruded by the ca. 811 Ma Dund ortho-complex (Bold et al., 2016a). These units are disconformably overlain by volcanic and siliciclastic rocks of the Yargait and Zavkhan fms. Rhyolite flows within the Zavkhan Formation (Fm) have been dated at 802.1 ± 1.0 Ma and 797.2 ± 1.1 Ma with U-Pb chemical abrasion-ion dilution thermal ionization mass spectrometry (CA-ID-TIMS) on zircon (Bold et al., 2016a). The Zavkhan Fm is unconformably overlain by the Khasagt Fm, which is composed of 0–2000 m of siliciclastic strata deposited in fault-bounded grabens, and Tsagaan-Olom Group, which consists of glacial diamictite and carbonate (Bold et al., 2016b).

The Tsagaan-Olom Group consists of the Cryogenian Maikhan-Uul, Taishir, and Khongor fms, and the Ediacaran Ol and Shuurgat fms (Figs. 1 and 2). Glacial diamictites and siliciclastic rocks of the Mai-khan-Uul Fm were deposited during the ~717–660 Ma Sturtian glaciation. The base of the overlying Taishir Fm has been dated with Re-Os on organic-rich lime-micrite at 659.0 ± 4.5 Ma, which is indistinguishable from dates on Sturtian cap carbonates at several localities globally (Rooney et al., 2015). The Taishir Fm is a 100–600 m thick limestone-dominated succession divided into four members (T1, T2, T3, and T4) that define the major sequence boundaries. The Taishir Fm is succeeded by glaciogenic deposits of the Khongor Fm, which ranges from 0 to 25 m thick and is composed of limestone clasts in weakly stratified shale, siltstone, and calcisiltite matrix. The Cryogenian Taishir and Khongor fms are sharply overlain by the Ol Fm, which hosts sedimentological features characteristic of basal Ediacaran cap dolostones

globally, including pseudomorphed aragonite fans, tubestone stromatolites, sedimentary barite, and giant wave ripples (Hoffman et al., 2011; Macdonald et al., 2009a). The Ol Fm is up to 40 m thick and is composed of buff-colored, finely-laminated micropeloidal dolostone (Ol cap dolostone), overlain by nodular bedded calcisiltite and flat-bedded lime-micrite interbedded with thin beds of shale, and massively bedded lime-grainstone.

The Ol Fm is conformably overlain by the Shuurgat Fm, which consists of up to 500 m of dolostone-dominated carbonate strata that is divided into four mappable members (Sh1, Sh2, Sh3, and Sh4). Above a karstic unconformity, the Shuurgat Fm is overlain by buff- to pink-colored stromatolitic dolostone, phosphatic shale, and thin-bedded limestone of the Zuun-Arts Fm (Smith et al., 2016). The main dolomitization event discussed in this study has affected the T3 and T4 members of the Taishir Fm and the entire Ol Fm.

During the Ediacaran Period, the southern margin of the Zavkhan Terrane transformed from a passive to an active margin. In the Lake Terrane, the Khantaishir ophiolite formed at ~571 Ma (Jian et al., 2014; Khain et al., 2003), and was obducted onto the Zavkhan Terrane by 545–520 Ma (Štípká et al., 2010). Throughout the Zavkhan Terrane, late Ediacaran to early Cambrian foreland deposits unconformably overlie the passive margin sequence (Smith et al., 2016). Accretion continued on the southern margin of the amalgamated Mongolian terranes throughout the Paleozoic and culminated with extensive Permian plutonism (e.g., Jahn et al., 2009).

3. Methods

3.1. Mapping of the transitions from dolomite to limestone

To better constrain the geometry and extent of dolomitization, we mapped the distribution of dolomitized carbonates in the Tsagaan-Olom Group for over 100 km along strike (Figs. 1 and 2). Transitions from limestone to dolostone within the Taishir Fm are easily traceable in the field due to a color contrast between the dark limestone and light dolostone (Figs. 3A–E). Excellent exposure and clear stratigraphic markers within the Taishir and Ol fms allowed us to follow specific stratigraphic horizons through dolomitization fronts (Figs. 3 and 4). Detailed mapping at the Taishir, Ol Mountain, and northern Bayan Gorge localities was carried out to document the transition from limestone to completely dolomitized carbonates (Fig. 2A). To characterize carbonate textures of the Taishir Fm, the Tsakhir Range (Fig. 2B) and Uliastai Gorge (Fig. 2C) exposures were mapped in detail. Additionally, the southern Khukh Davaa section (Fig. 2D) was mapped in detail to document the relationship between the dolomitization fronts and bedded barite at the top of the Ol cap dolostone. The Shuurgat Fm carbonates were also studied in detail in Khongor Range (Figs. 2A – F708, F947, and U1439) and in Khunkher Gorge (Fig. 2C – F872 and U1437) to further assess the significance of a subsequent dolomitization event responsible for the rest of the Tsagaan-Olom Group carbonates. In each of these localities, Bold et al. (2016b) documented both vertical and along strike transitions from limestone to dolostone from representative stratigraphic sections of the Taishir Fm.

3.2. Isotopic analysis – $\delta^{13}\text{C}$, $\delta^{18}\text{O}$, $\delta^{44}\text{Ca}$, and $\delta^{26}\text{Mg}$

The studied sections of the Taishir and Ol Fm carbonates (Fig. 5) were sampled at ~1 m resolution for $\delta^{13}\text{C}$ and $\delta^{18}\text{O}$, at 3–4 m for $\delta^{26}\text{Mg}$ and $\delta^{44}/\delta^{40}\text{Ca}$ analysis (Table S1), and splits of the same micro-drilled sample powders were used in each analysis. Shuurgat Fm carbonates (Fig. 6) were sampled at 2–3 m resolution for $\delta^{13}\text{C}$ and $\delta^{18}\text{O}$ analysis. Powders were drilled from the freshest carbonate with minimal cleavage, siliciclastic components, and veining (Figs. 7–9). Approximately 1400 samples were analyzed for $\delta^{13}\text{C}$ and $\delta^{18}\text{O}$, while 144 were analyzed for $\delta^{44}/\delta^{40}\text{Ca}$ and $\delta^{26}\text{Mg}$. Methods for $\delta^{13}\text{C}$ and $\delta^{18}\text{O}$ analysis are described in Bold et al. (2016b). Data are reported in mil (‰)

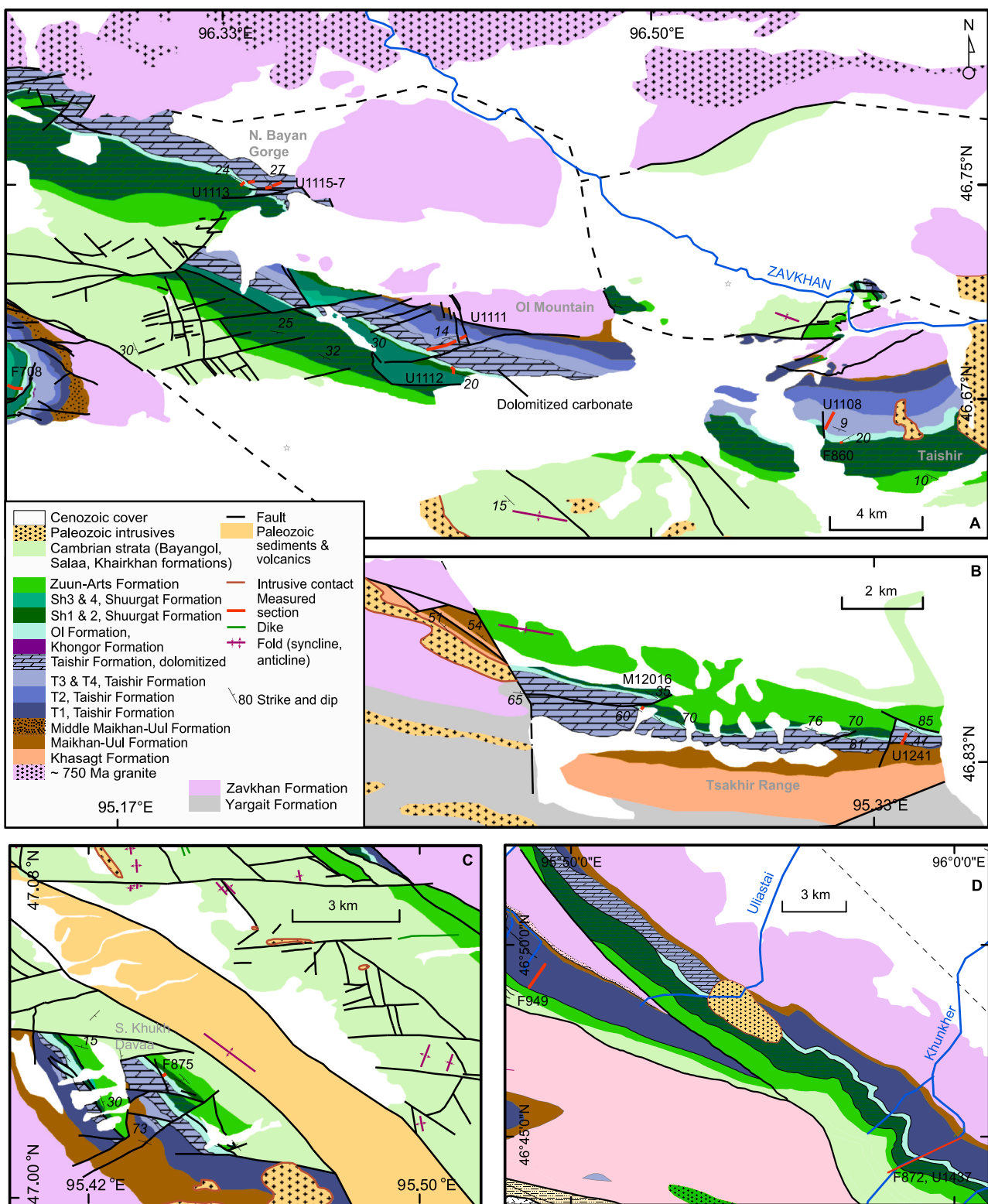


Fig. 2. Detailed geological maps. A) Geological map of the Taishir, Ol Mountain, and northern Bayan Gorge localities. Mapped transition from dolomite to limestone is shown by dolomite symbol. The Taishir locality hosts non-dolomitized Taishir (except a few meters of partially dolomitized carbonates in the upper T3) and upper OI Formation carbonates. Dolomitization becomes more pervasive and expansive to the northwest and the uppermost Taishir and the entire OI Formation carbonates are dolomitized in Ol Mountain. The whole T3 including upper T2 of the Taishir Formation as well as the entire OI Formation is dolomitized in northern Bayan Gorge. B) Geological map of the Tsakhir Range. Taishir Formation carbonates are completely dolomitized here except the basal T1 limestone. Upper OI Formation carbonates are also dolomitized. C) Geological map of southern Khukh Davaa. Dolomitized carbonates are highlighted. D) Geological map of Khunkher Gorge. The entire Taishir Formation is non-dolomitized. Member Sh3-4 of the Shuurgat Formation is dominated by limestone.

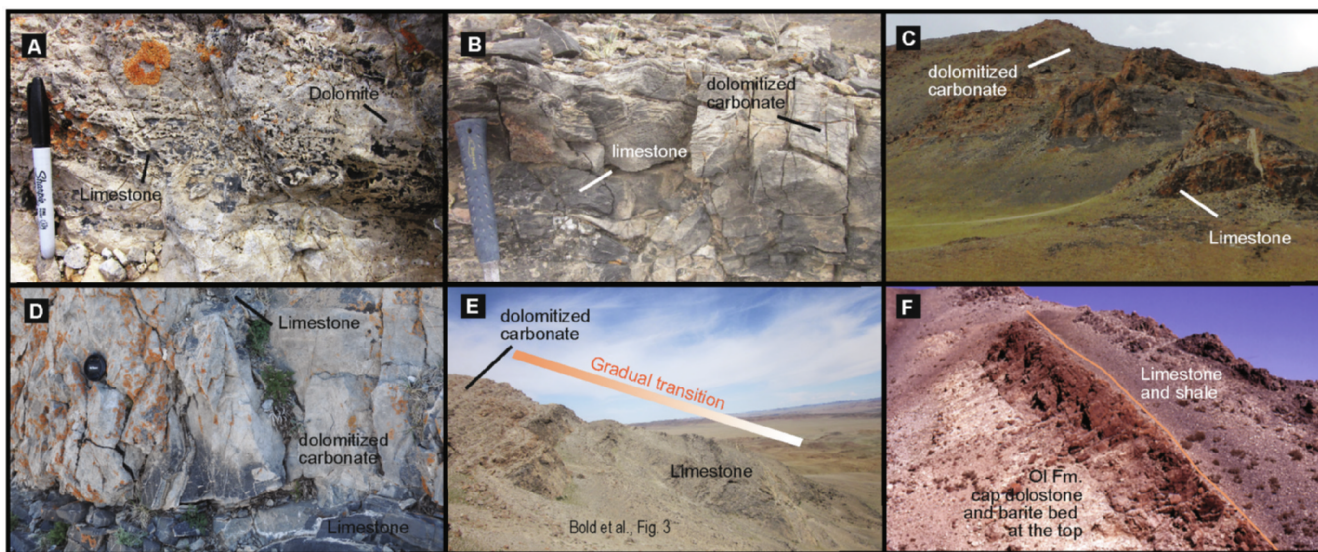


Fig. 3. Dolomitization fronts. Localities are labeled on Fig. 1 and described in Bold et al. (2016a,b). A) Member T3 irregularly dolomitized carbonate in northwestern Tsakhir Range. B) Partial dolomitization in Member T3 (section U1108) at Taishir. C) Dolomitized T3 carbonates at southern Khukh Davaa. Contact between dolomite and limestone is irregular. D) Dolomitized Taishir carbonates at Unkheltseg Range. Contact between dolomite and limestone is diffuse. E) Dolomitized upper T3 carbonates at Ol Mountain. Contact between dolomite and limestone is gradual. F) Sharp transition from Ol Formation cap dolostone to limestone overlain by recessive shale (section F875) at southern Khukh Davaa. ~10 cm thick-bedded barite is marked with orange line. (For interpretation of the references to color in this figure legend, the reader is referred to the web version of this article.)

notation relative to the standard VPDB with a precision of 0.01–0.05‰.

For $\delta^{26}\text{Mg}$ and $\delta^{44/40}\text{Ca}$ analysis, ~5 mg powder was dissolved in ~5 mL 0.1 M buffered acetic acid. Before processing them using an automated Thermo Dionex 5000+ ion chromatography (IC) system, sample solutions were ultra-sonicated for 3–4 h to aid full dissolution of the carbonate fraction. The sample solution was then processed through the IC system using a CS16 cation exchange column that separates and collects pure Ca or Mg cuts based on peak intensities measured from changes in conductivity. Collected fractions were dried completely and then treated with 200 microliters (μL) of concentrated nitric acid (16 N HNO_3). After being dried again, the samples were re-dissolved in 2% HNO_3 in preparation for isotope analysis.

Both $\delta^{44/40}\text{Ca}$ and $\delta^{26}\text{Mg}$ values were determined using a Thermo Neptune Plus inductively coupled plasma mass spectrometer (MC-ICP-MS) at Princeton University. Analyses were in medium-resolution mode for Ca and low-resolution mode for Mg using sample-standard bracketing methods to correct for instrumental mass bias. For Ca isotope analysis, all of the samples were diluted to 2 ppm Ca in 2% HNO_3 , with sample concentrations matching standard concentrations to within 0–10% to decrease concentration-dependent isotope effects and ensure comparable levels of ArHH^+ interference across samples and standards. Measured $\delta^{42/40}\text{Ca}$ values are converted to $\delta^{44/40}\text{Ca}$ values relative to modern seawater assuming mass dependent fractionation with a slope of 2.05. The long term external reproducibility is determined based on the standard deviation of known standards with SRM915b measured to $-1.19 \pm 0.14\text{\textperthousand}$ (2σ , $N = 120$) and SRM915a measured to $-1.86 \pm 0.16\text{\textperthousand}$ (2σ , $N = 24$). For Mg isotope analysis, all samples were diluted to 150 ppb Mg in 2% HNO_3 , with sample concentrations matching standard concentrations to within 0–20%. $\delta^{26}\text{Mg}$ values are reported in delta notation relative to Dead Sea Metal (DSM-3) and the long-term external reproducibility for Cambridge-1 is $-2.61 \pm 0.10\text{\textperthousand}$ (2σ , $N = 81$) and Seawater is $-0.83 \pm 0.10\text{\textperthousand}$ (2σ , $N = 47$). Every sample was measured twice within the same run on the mass spectrometer. Further details of Ca and Mg isotope analysis as well as the IC system are described in Husson et al. (2015) and Blättler et al. (2015).

In order to further document small-scale geochemical variability, different textures were micro-drilled for $\delta^{13}\text{C}$ and $\delta^{18}\text{O}$ analysis.

Textures were distinguished based on visible comparison of crystal size and color and up to 5 different regions were micro-drilled in each hand-specimen. These textures are described in Table S2 and texture 1 is the original micro-drilled carbonate used to construct composite $\delta^{13}\text{C}$ curve for the Tsagaan-Olom Group carbonates in Fig. 1C. Isotopic values of the other textures are shown on Figs. 8 and 9 to highlight isotopic variability preserved in a single hand-specimen.

3.3. Petrography

Thin sections were made from 17 selected samples (U1108-47, 55.7, 60, 66; U1111-60.5, 71, 85, 94, 116; U1115-26, 44; U1116-162; U1117-188; U1110-1; U1112-5.4, 20.2, 23) for petrographic examination. Both primary and replacement textures were described and documented (Fig. 7) after Folk (1965) and compared with the stable isotopic variability. Selected samples were stained by Alizarin red and Potassium Ferricyanide composite (Evamy, 1963; Tamer, 1965) for differentiation of calcitic and dolomitic fabrics.

Carbonates textures were described as fabric-retentive if both depositional (Sander, 1951) and early diagenetic constituents (Lucia, 1995) were preserved, and fabric-destructive if the primary carbonate constituents were heavily-recrystallized, while post-depositional features such as veins (Antonellini, 2000) and breccias (Blount and Moore, 1969) might still be preserved. Retention and destruction of bedding refer to the preservation state of primary bedding characteristic of each unit.

3.4. Fluid inclusions

Carbonate-hosted fluid inclusions were studied to help discriminate various dolomitization models. Doubly polished thin sections (100 μm thick) from the same limestone and dolostone slabs used for isotopic and elemental analyses of the Taishir and Ol fms were used. Samples were selected from the three parallel sections in Taishir (U1108-10 – Taishir Fm limestone; F860-5.5 – Ol Fm cap dolostone), Ol Mountain (U1111-65, 172 – Taishir Fm dolostone; U1112-14.6 – Ol Fm cap dolostone; U1112-36.5 – Ol Fm dolostone) and northern Bayan Gorge (U1115-81, U1116-82.1, U1117-36 – Taishir Fm dolostone; U1113-8.8

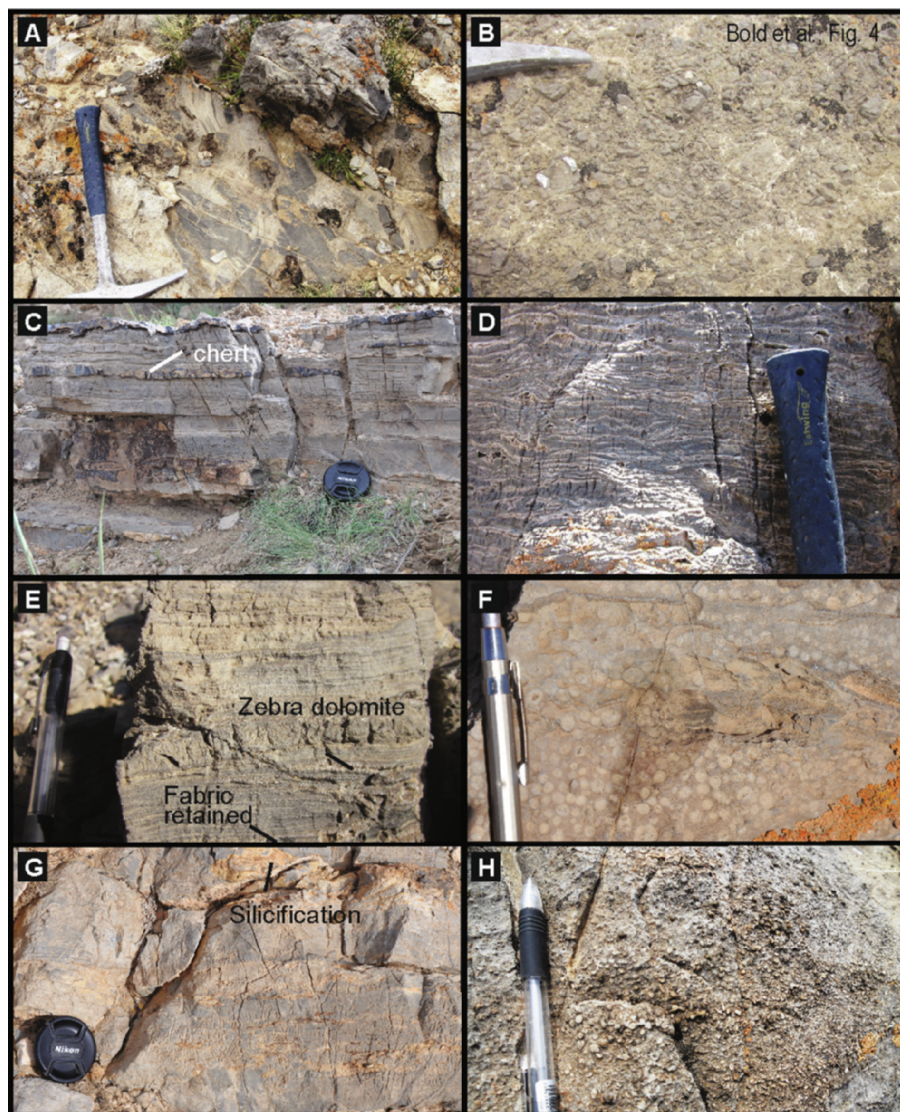


Fig. 4. Dolomitized carbonates of the Taishir, Ol, and Shuurgat formations. Localities are labeled on Fig. 1 and described in Bold et al. (2016a,b). A) Irregular dolomitization in the partially dolomitized T3 at Ol Mountain B) Brecciated Taishir carbonate at Unkheltseg Range. C) Dolomitized basal T3 (section U1115) at northern Bayan Gorge. The resistant bed-parallel lenses are chert. Camera lens cap for scale is 52 mm in diameter. D) Texture destructive dolomite, zebra dolomite, which is intensively recrystallized with abundant bed parallel veins (stratigraphic section U1115-26 m) at northern Bayan Gorge. E) Zebra dolomite in Sh2 at Ol Mountain. In the lower left, fabric-retained dolomite is preserved and characterized by thinly laminated beds of carbonate. Pencil for scale is 15 cm. F) Ooid dolo-grainstone of Sh3 at Khongor Range (Section F708). Pen for scale is 10 cm. G) Massively weathered and silicified dolomicrite of Sh4 of the Shuurgat Formation in Khongor Range. H) Dolomitized and silicified ooid-grainstone in T3, northern Khukh Davaa. Pen for scale is 12 cm.

– Ol Fm cap dolostone; U1113-43 – Ol Fm dolostone) (Fig. 5). As an external comparison, 6 doubly-polished thin sections were made from the Marinoan cap carbonate (the Keilberg Member; Hoffman et al., 2011) from Namibia. Petrographic observations were made (Fig. S1 and Table S3) in both transmitted and reflected lights using a Nikon eclipse EL 100 N POL microscope. Fluid inclusion microthermometry was undertaken using a Linkam THMS 600 heating-freezing stage (with Olympus 50 \times long focus lens) at the International Center for Research and Education on Mineral and Energy Resource, Akita University in Japan. The thermocouple for the heating/freezing stage was calibrated using melting temperature of metals and the ice melting temperature of pure water. The homogenization temperature (T_h) has a calibration error of < 1 °C, whilst the accuracy of ice melting is ± 0.1 °C. A 1 °C/min heating rate was applied to all heating and cooling experiments. Analyzed inclusions were between 2 and 8 μm in length. Fluid inclusion types at room temperature, size of inclusions, T_h , and final ice melting temperature measurements were obtained. Salinity was determined by ice melting and solid melting temperatures (Bodnar, 1993) and reported as wt% (NaCl eq.) (Table S3).

3.5. Elemental concentration

Splits from the micro-drilled sample powders that were used for isotopic analysis (Fig. 5) were used for elemental concentrations. A

total of 173 representative carbonate samples of the Taishir and Ol fms from sections measured in Taishir (U1108, F860), Ol Mountain (U1111, U1112), and northern Bayan Gorge (U1113, U1115-7) and 27 samples of the Shuurgat Fm from the Khongor Range (F708 and U1439) were analyzed (Figs. 5 and 6; Table S1). Concentrations of Mn, Sr, Mg, and Ca were measured on a Thermo Scientific Element 2 and a Thermo Finnigan iCAP Q Inductively Coupled Plasma Mass spectrometer (ICP-MS) at Princeton University. Because the samples were dissolved in 0.1 M buffered acetic acid, which leaves the insoluble silicate fraction behind, the elemental compositions are assumed to reflect that of the carbonate fraction. For the analysis, 25 μl of sample solution was diluted in 1 ml (mL) of 2% HNO_3 acid and measured against six in-house multi-element standards. All of the data are reported in ratios relative to Ca. The external reproducibility of the ratios is < 10% based on replicate measurements of SRM88b ($N = 29$).

4. Results

4.1. Extent of dolomitization on the Zavkhan Terrane

At the Taishir (Figs. 2A and 5C) and Uliastai Gorge (Figs. 2D and 5F) localities, the entire Taishir Fm is preserved predominantly as limestone. Elsewhere members T1 and T2 are typically preserved as limestone while dolomitization is pervasive in the overlying units, with the

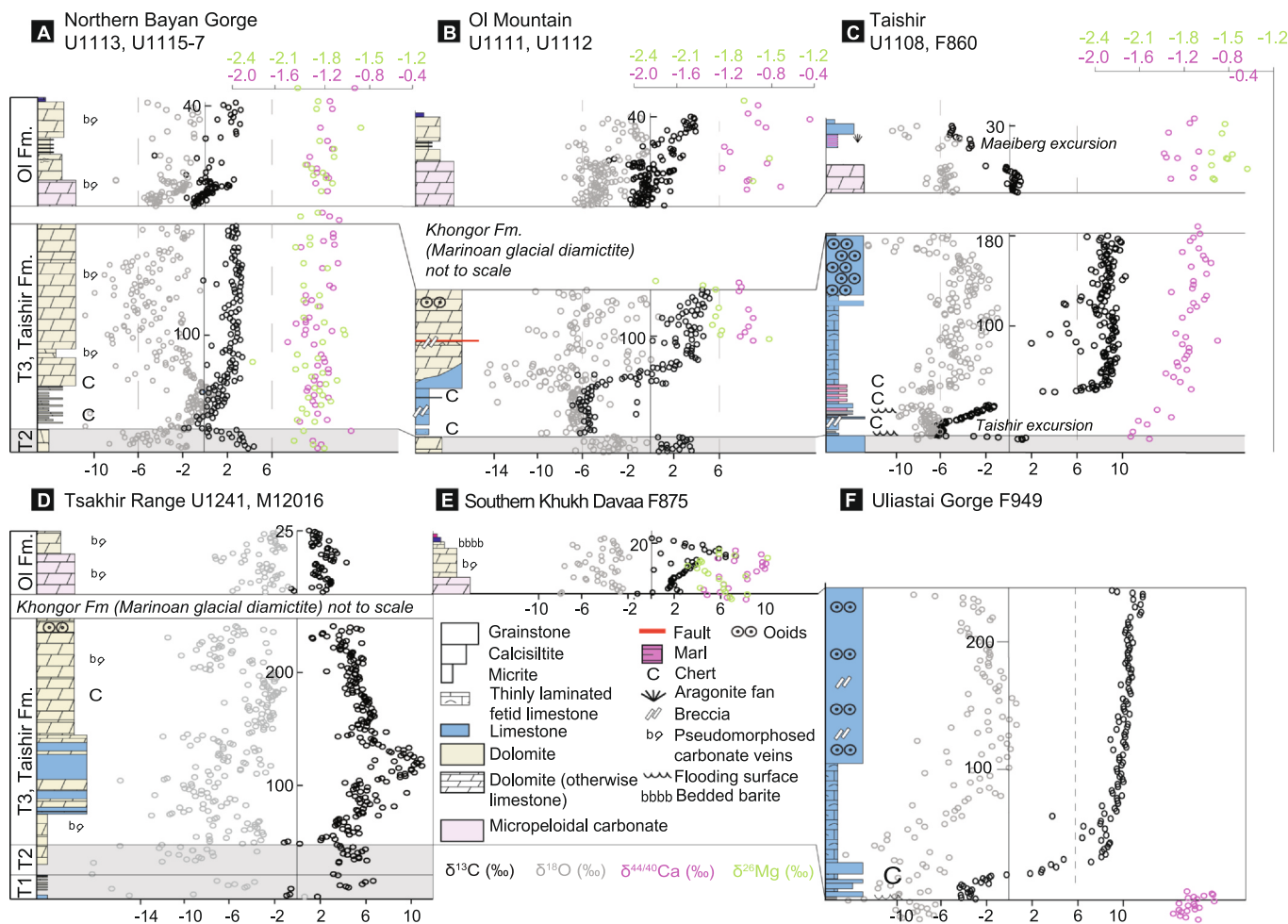


Fig. 5. Chemostratigraphy of the Taishir and Ol formations at: A) northern Bayan Gorge, B) Ol Mountain, C) Taishir, D) Tsakhir Range, E) southern Khukh Davaa, and F) Uliastai Gorge. The Khongor Formation thickness is not drawn to scale. Carbonate successions that are not directly related to the main dolomitization event are excluded or marked in grey.

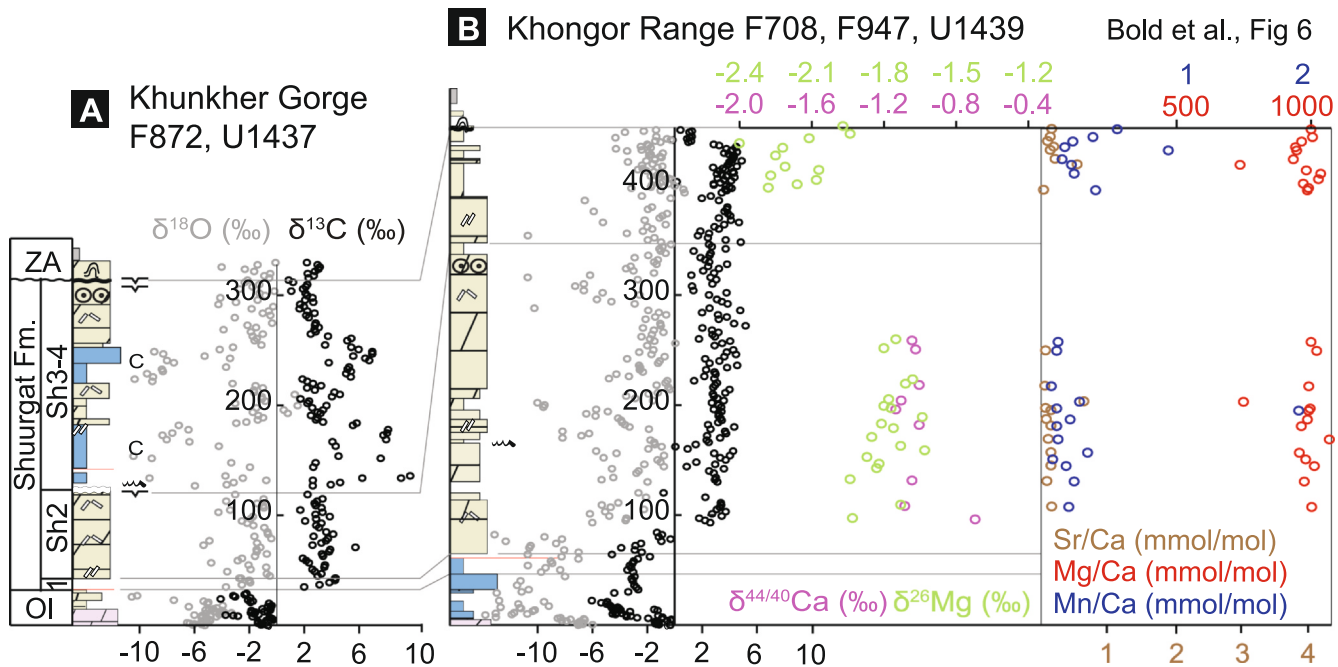


Fig. 6. Chemostratigraphy of the Shuurgat Formation at A) Khunkher Gorge and B) Khongor Range. Legend for lithology is in Fig. 5. Detailed description of the Ol Formation exposed at these localities are in Bold et al. (2016b).

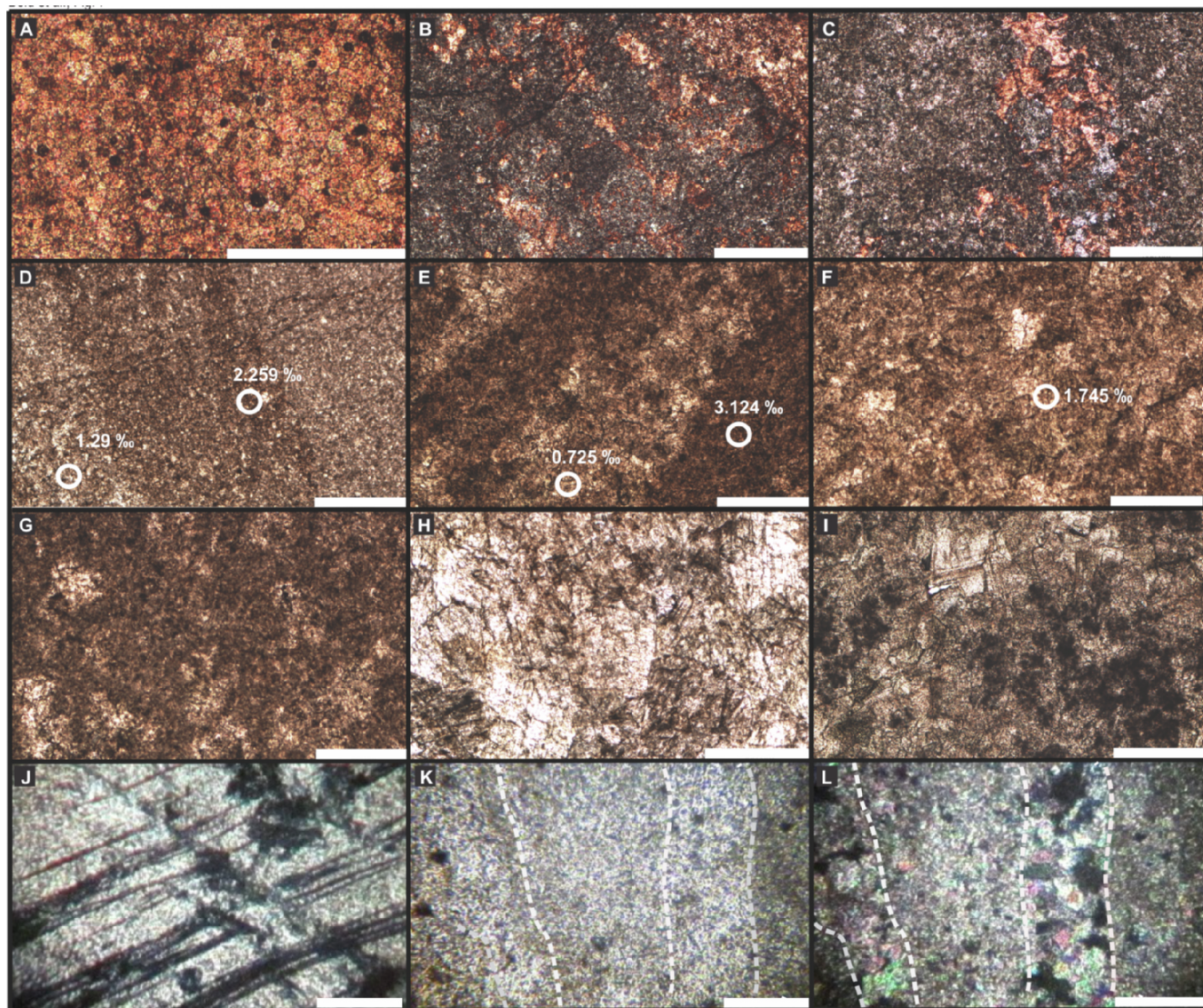


Fig. 7. Photomicrographs of carbonate textures from the Taishir and Ol formations. White horizontal bars for scale are 500 μm in length. A, B, and C are Alizarin red and Potassium Ferricyanide stained carbonates where the limestone phases appear red. A) Fine-crystalline T3 limestone from the Taishir locality (U1108-60 m, Fig. 4). Irregular dolomitization in the partially dolomitized T3 from Ol Mountain (B; U1111-71 m) and northern Bayan Gorge (C; U1116-162 m). D-F) Texture dependent variable $\delta^{13}\text{C}$ values from U1111-71 m (D) and U1111-94 m (E-F) of the Ol Mountain section. Dark brown anhedral carbonates preserve higher $\delta^{13}\text{C}$ values whereas subhedral to anhedral, light grey carbonates preserve lighter $\delta^{13}\text{C}$ values. G-H) Medium to coarse-crystalline and subhedral to euhedral dolomite representative of completely dolomitized T3 from northern Bayan Gorge section U1117-188 m (G) and Ol Mountain section U1111-70-saddle dolomite (H). I) Ol cap dolostone from Taishir locality (F860). The carbonates are mm-laminated and composed of interbeds of microcrystalline, anhedral, and cloudy dolomite and subhedral to euhedral, coarse-crystalline, and clear dolomite. J) Bedded barite (in cross-polarized light) of the Ol Formation as preserved above the Marinoan Ol cap dolostone at southern Khukh Davaa. K-L) Carbonatized veins (outlined by dashed lines) depicting barite pseudomorphs (K in plane-polarized light, L in cross-polarized light) in dolomite matrix. (For interpretation of the references to color in this figure legend, the reader is referred to the web version of this article.)

exception of < 1 m thick dolostone beds in the upper portion of T2 (Bold et al., 2016b). Dolomitization fronts often display irregular contacts with the limestone beds underneath (Figs. 3B–E) with halos of partially dolomitized limestone extending tens of meters around completely dolomitized zones. Some contacts between limestone and dolostone are more sharply defined, such as that at the top of the Ol Fm (Fig. 3F); however, these appear to correspond with stratigraphic boundaries and thus likely differences in original porosity.

Transitions from dolomite to limestone are discontinuous across block bounding faults (Figs. 1, 2A and C). Many of these are Paleozoic right-lateral faults, and the transitions from dolomite to limestone across individual blocks can be used as a piercing point to restore fault offset, demonstrating that the dolomitization largely predates faulting. However, some of these faults are likely reactivated Precambrian faults. Particularly, an Ediacaran fault on the Zavkhan Terrane (Bold et al.,

2016b) is suggested by the erosion of the Member Sh4 and the presence of a well-defined sandstone-filled karst at the top of the Shuurgat Fm in southern Khukh Davaa, Tsagaan, and a portion of the Khunkher blocks (Bold et al., 2016b). This boundary also coincides with a jump in the stratigraphic locus of dolomitization from predominantly within Taishir Fm to up into both the Taishir and Shuurgat fms.

The basal Ol Fm is identified as the Marinoan cap dolostone (Ol cap dolostone, Macdonald et al., 2009a) and is preserved as dolostone on the Zavkhan Terrane (Bold et al., 2016b). Where the underlying Taishir Fm is limestone, the lime-grainstone unit of the upper Ol Fm is also preserved as limestone (Fig. 5C). These localities coincide with the distribution of the shale matrix diamictite of the Khongor Fm, which separates the Taishir and Ol fms. In contrast, in localities where the underlying Taishir Fm is dolomitized the lime-grainstone unit of the upper Ol Fm is preserved as dolostone.

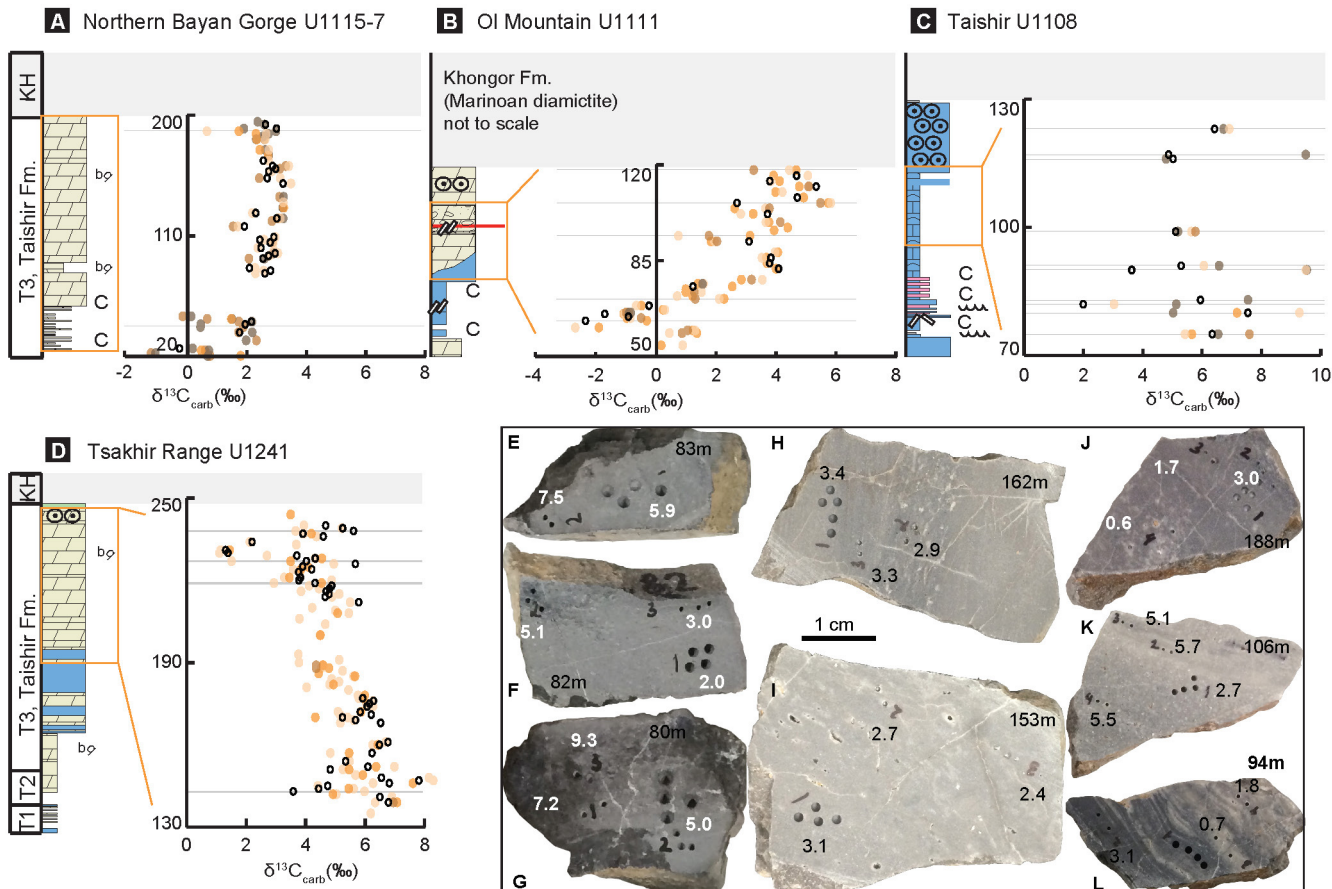


Fig. 8. Isotopic variability recorded in hand samples of the Taishir Formation. Interval of examination is boxed in orange. Black circles denote whole-rock analyses included in original $\delta^{13}\text{C}$ profiles shown in Fig. 5. Orange-filled circles denote micro-sampled textures analyzed to investigate isotopic variability. Intervals with $\geq 2\text{\textperthousand}$ are highlighted with grey horizontal lines. Selection of hand samples that preserved variable isotopic values is shown in the box. E–G – U1108, H–I – U1116, J – U1117, and K–L – U1111. Stratigraphic height of each sample is labeled in meters. (For interpretation of the references to color in this figure legend, the reader is referred to the web version of this article.)

In the Taishir locality (Figs. 2A and 5C), both the Taishir and upper Ol fms are composed of limestone. Partially dolomitized carbonates are present in the upper portion of T3 (Fig. 3B). From the Taishir locality, dolomitized carbonates expand northwest along strike towards Ol Mountain (~11 km from Taishir locality; Figs. 2A and 5B) where the upper portion of T3 (Figs. 3C–E, 4A, and B) and the upper portion of the Ol Fm are completely dolomitized. At Ol Mountain, the basal Ol Fm also preserves abundant secondary veins. Further along strike, at northern Bayan Gorge, the dolomitization front expands to replace the upper portion of T2, the entirety of T3 (Fig. 4D), and the Ol Fm (Fig. 5A). In northern Bayan Gorge, the Ol Fm also contains abundant secondary veins, which are common at the most pervasively dolomitized localities.

Further west and southwest on the Zavkhan Terrane, both the upper Taishir and Ol fms are preserved as dolostone and secondary carbonate veins become more abundant. In Tsakhir Range (Fig. 2B) and at southern Khukh Davaa (Fig. 2C), progressive fabric destruction is displayed (Fig. 3A), where relict limestone, dark grey in color, is surrounded by pale brown coarse crystalline dolomite. Similarly, in the Tsakhir Range, the transition from dolomite to limestone is laterally discontinuous forming lenticular bodies.

The Ol Fm contains abundant secondary carbonate veins and dolomitization remobilized barite. At southern Khukh Davaa (Figs. 2C, 3F, and 5E), below the < 20 cm thick bedded barite (Fig. 7J), carbonatized barite veins are common. Petrographic observations of the veins display barite pseudomorphs that are replaced by carbonate (Fig. 7K–L). Similar veins are found in the underlying Taishir Fm and are also composed of dolomite.

Where exposed, the basal Shuurgat Fm, Sh1, is composed of fine- to medium-bedded lime-micrite interbedded with marly shale and calcisiltite. The rest of the Shuurgat Fm is dominated by dolostone (Fig. 4E–H) except Sh3–4 in Khunkher (Fig. 6A) and Tsagaan gorges (Bold et al., 2016b). Limestone of the Member Sh1 is well exposed in Khongor Range (Figs. 2A and 6B); however, the transition from limestone to dolostone is impeded by a small fault and a few meters of non-exposure. In Khongor Range, Sh2, Sh3 and Sh4 are all pervasively dolomitized. In contrast, at Khunkher Gorge (Figs. 2D and 6A) Sh3 and Sh4 is predominantly preserved as limestone and rests on a karstic unconformity at the top of Sh2 (Bold et al., 2016b). Secondary carbonate veins exhibited in Sh2 are characterized as zebra dolomite (Fig. 4E; Diehl et al., 2010; Lugli et al., 2000; Swennen et al., 2003; Vandeginste et al., 2005 and references therein) and although it is a useful map unit, it may not represent a correlative sequence stratigraphic unit. In general, the Shuurgat and Ol fms are more commonly dolomitized than the Taishir Fm.

Silicification is common in dolomitized carbonate of the Taishir, Ol, and Shuurgat fms. It is prevalent in the upper portion of T3 of the Taishir Fm (Fig. 5 – Tsakhir Range) and dramatically displayed in silicified ooids that are resistant to weathering (Fig. 4H). In the Ol Fm, dolomitized aragonite fans in the Ol Fm are also silicified. Dolomitized Sh3–4 carbonates preserve both primary chert nodules that are sometimes bedded to lenticular and secondary silicification seams (Fig. 4G). Karsted surfaces present above Sh2 in Khunkher Gorge and at the top of the Shuurgat Fm are also silicified (Bold et al., 2016b).

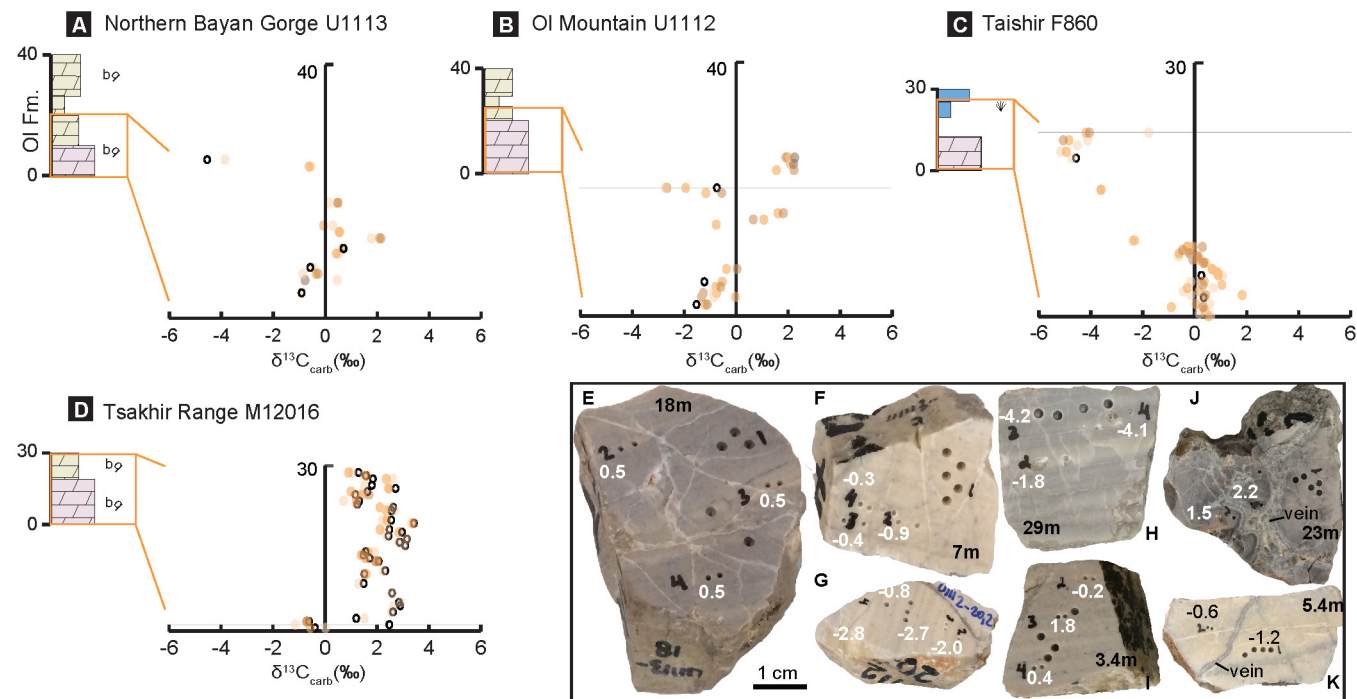


Fig. 9. Isotopic variability recorded in the Ol Formation carbonates in hand sample scale. Legend is in [Fig. 8](#). Selection of hand samples that preserved variable isotopic values is shown in the box. E-F – U1113, G and J-K – U1112, and H-I – F860. Stratigraphic height of each of the samples is labeled in meter.

4.2. Texture and petrography

An array of paragenetic and diagenetic textures and structures are developed in the dolomitized carbonates. Destruction of primary features becomes more apparent as dolomitization becomes more pervasive.

4.2.1. Preservation and destruction of bedding

In the dolomitized T3 carbonates of the Taishir Fm, primary bedding is best preserved at northern Bayan Gorge ([Fig. 4C](#)) where the typical basal T3 fine- to medium-bedded micrites with bedded cherts are still preserved. In the limestone equivalent sections, the upper T3 is defined by thinly laminated and fetid limestone mudstone ([Bold et al., 2016b](#)); however, bedding is never preserved in the dolomitized sections and the upper T3 instead consists of heavily brecciated, veined, and recrystallized massive dolomite ([Figs. 4A-B and D](#)). The characteristic fine lamination of the Marinoan cap dolostone ([Macdonald et al., 2009a](#)) of the basal Ol Fm is preserved at the Taishir locality where the underlying Taishir Fm is minimally dolomitized. Elsewhere, where the underlying Taishir Fm is heavily dolomitized, the overlying Ol Fm is brecciated and veined.

4.2.2. Retention and destruction of carbonate fabrics

Upper T3 of the Taishir Fm is characterized by ooid-grainstone in limestone successions and the ooids are preserved in dolomitized equivalents and are commonly silicified ([Fig. 4H](#)). The sequence of fabric destruction is nicely demonstrated in transitional zones from limestone to dolostone in southern Khukh Davaa ([Fig. 3C](#)) where primary textures can be observed from relict limestone. Elsewhere, in the upper portion of T3, as dolomitization becomes pervasive, carbonate successions get massively recrystallized and in extreme cases, form extensively veined, coarse-crystalline, vuggy, sugary, and brecciated dolomites ([Figs. 4A-B](#)) and zebra texture ([Fig. 4D](#)). These are uncommon in the upper Ol Fm dolostone. Secondary carbonate veins and coarse-crystalline dolomite are the main features of the dolomitized upper Ol Fm. In Sh2 and upper Sh3-4, heavily recrystallized dolomites are prevalent in massively bedded units of the Shuurgat Fm but vuggy

and brecciated textures are almost absent. In addition to the preservation of the fine bedding of the Sh2, ooids are well-preserved in the Sh3 ([Fig. 4F](#)).

Microscopic textures of the Taishir Fm vary from fine-coarse crystalline and subhedral-euhedral dolomite, often associated with variable $\delta^{13}\text{C}$ values ([Section 4.3](#)), to nonplanar, fine crystalline, and anhedral limestone, which preserves the very positive $\delta^{13}\text{C}$ values. These limestone textures consist of nonplanar anhedral to subhedral crystals, which are well illustrated in thin sections of the lower T3 thin-bedded lime-micrite sampled in the Taishir locality ([Fig. 7A](#)). Along strike, those rocks become first partially dolomitized ([Figs. 7B-E](#)) and then completely dolomitized ([Figs. 7F-I](#)), as best illustrated in samples from the Ol Mountain and northern Bayan Gorge localities. Saddle dolomite ([Radke and Mathis, 1980](#)), which is characteristic of a burial dolomitization regime, is not common in the dolomitized carbonates of both Taishir and Ol fms but is preserved at the top of the Taishir Fm at Ol Mountain ([Fig. 7H](#)).

4.3. Isotopic results – $\delta^{13}\text{C}$, $\delta^{18}\text{O}$, $\delta^{44}\text{Ca}$, and $\delta^{26}\text{Mg}$

4.3.1. $\delta^{13}\text{C}$ and $\delta^{18}\text{O}$

Limestone successions: At the Taishir locality ([Fig. 5C](#)), the Taishir and Maieberg negative carbon isotope ($\delta^{13}\text{C}$) excursions ($> -6\text{\textperthousand}$; [Macdonald et al., 2009a](#)) are well preserved in limestone successions of the Taishir and Ol fms, respectively. Similarly, the prolonged positive $\delta^{13}\text{C}$ values (+8 to +9‰) recorded in the T3 above the Taishir excursion are well-preserved ([Bold et al., 2016b](#)). $\delta^{18}\text{O}$ values in the Taishir Fm vary from -1.0 to $-10.1\text{\textperthousand}$ throughout without any apparent covariance with $\delta^{13}\text{C}$. Internal variability within each unit is greatest in the upper T3, which is characterized by massively bedded lime-grainstone with abundant ooids at the top. In the Ol formation, $\delta^{18}\text{O}$ values are consistently low -5 to $-11\text{\textperthousand}$ and do not correlate with the Maieberg negative $\delta^{13}\text{C}$ excursion.

The Ol Mountain locality ([Fig. 5B](#)), which is located along strike of the Taishir locality ([Fig. 2A](#)), preserves limestone in the lower portion of T3. In this locality, the Taishir Fm contains both the negative $\delta^{13}\text{C}$ excursion and the positive (+8 to +9‰) excursion in the overlying

strata. $\delta^{18}\text{O}$ values vary from +1 to -14‰ with no covariance with $\delta^{13}\text{C}$.

Lithostratigraphically, carbonates from the Uliastai Gorge locality (Fig. 5F) have a similar appearance to carbonates from the Taishir locality and also preserve the Taishir negative $\delta^{13}\text{C}$ excursion and the positive $\delta^{13}\text{C}$ values (+8 to +9‰) in the strata above. However, the Taishir negative $\delta^{13}\text{C}$ excursion is expressed at the minimum of -4‰, which is ~2‰ lower than the nadir at the Taishir locality (Fig. 5C). Similar to the Taishir locality, $\delta^{18}\text{O}$ values do not correlate with $\delta^{13}\text{C}$ values, but reach values as low as -14‰ in the basal T3.

Partially dolomitized carbonates are preserved between 75 and 125 m in section U1108 (Taishir locality, Fig. 5C) and 75–140 m in section U1241 (Tsakhir Range, Fig. 5D). In these intervals, the respective $\delta^{13}\text{C}$ values decrease to ~+2‰ in U1108 and to +3 to +4‰ in U1241 without much variability in $\delta^{18}\text{O}$.

Dolomitized successions: At Ol Mountain, the prolonged positive $\delta^{13}\text{C}$ values of the dolomitized uppermost Taishir Fm reach up to +5‰ (Fig. 5B), which are significantly lower than the ~+10‰ values recorded in equivalent limestone strata at the Taishir locality. At the third parallel section measured at northern Bayan Gorge (Fig. 5A), where the entire Member T3 carbonates are dolomitized, the Taishir negative $\delta^{13}\text{C}$ excursion is barely present (>-2‰) and the $\delta^{13}\text{C}$ values in the overlying dolomitized carbonate only increases to a maximum of +3‰. A similar pattern is recorded in $\delta^{13}\text{C}$ values of the Tsakhir Range section, where the nadir of the Taishir excursion reaches only ~-2‰ (Fig. 5D).

$\delta^{18}\text{O}$ values of the dolomitized Taishir Fm are highly variable in each section and display no covariance with the respective $\delta^{13}\text{C}$ trend (Fig. 5). $\delta^{18}\text{O}$ values range from +1 to -10‰ at northern Bayan Gorge, but become even lighter, <-14‰, at Ol Mountain and the Tsakhir Range sections.

$\delta^{13}\text{C}$ values of the Ol cap dolostone successions at the three parallel sections, the Taishir, Ol Mountain, and the northern Bayan Gorge (Figs. 5A-C), are all at ~0‰, but internal variability is greater in Ol Mountain and northern Bayan Gorge. $\delta^{18}\text{O}$ values of the Ol cap dolostone in the Taishir locality are at ~-6‰ and become heavier and more variable along strike to the west and reach as high as ~0‰ at Ol Mountain and northern Bayan Gorge. In contrast, $\delta^{13}\text{C}$ values of the Ol cap dolostone successions in the Tsakhir Range (M12016; Fig. 5D) and southern Khukh Davaa (F875; Fig. 5E) are at ~+2‰. At these localities, $\delta^{18}\text{O}$ values are more variable and range from -1 to -10‰.

The Maieberg negative $\delta^{13}\text{C}$ excursion (Fig. 5C), which is preserved in limestone of the upper Ol Fm at the Taishir locality, is lost in the equivalent dolomitized strata. $\delta^{13}\text{C}$ values start at -2‰ and reach +4‰ in Ol Mountain (Fig. 5B). Along strike in northern Bayan Gorge, $\delta^{13}\text{C}$ values reach as high as +3‰ from -2‰ (Fig. 5A). Further to the west and northwest $\delta^{13}\text{C}$ values stay high and reach ~+4‰ in the Tsakhir Range (Fig. 5D) and ~+7‰ in southern Khukh Davaa (Fig. 5E). $\delta^{18}\text{O}$ values in dolomitized upper Ol Fm carbonates range from ~-6 to 0‰ at all localities (Fig. 5) but are consistent lowest at the Taishir locality (Fig. 5C).

The Shuurgat Fm carbonates: In Khunkher Gorge (Fig. 6A), the base of the Shuurgat Fm (Sh1) is not present due to a local fault and the entire succession starts with Sh2 dolomites with $\delta^{13}\text{C}$ values at ~+3‰. Above the major karsted surface at the top of the Sh2, a few meters of limestone are preserved in Sh3-4. These limestones preserve very positive $\delta^{13}\text{C}$ values that range from +2 to +10‰ while values return to +3‰ in the dolomitized equivalents in the middle. In the limestone successions, $\delta^{18}\text{O}$ isotopes reach as low as -10‰ compared to the dolomitized strata with values ranging from ~+2 to -6‰.

In the Khongor Range (Fig. 6B), no limestone is preserved in the Sh3-4, but the Sh1 is exposed and composed of limestone. The $\delta^{13}\text{C}$ signature of Sh1 is characterized by negative values with values as low as -2.7‰. The rest of the Shuurgat Fm carbonates are all dolomitized (Figs. 4F-G) and the $\delta^{13}\text{C}$ values stay at ~+3‰ with a minimum at -0.8‰ and maximum at +5.2‰. This signature changes to less

enriched values of +1‰ in the basal Zuun-Arts Fm (Smith et al., 2016). $\delta^{18}\text{O}$ values of the Shuurgat Fm at this locality are between -13 and +1‰ and covary with the $\delta^{13}\text{C}$ trend.

Isotopic variability in hand sample scale: >2‰ variability in $\delta^{13}\text{C}$ is uncommon in co-existing calcite and dolomite (Degens and Epstein, 1964). However, we observed >2‰ variability in $\delta^{13}\text{C}$ values within 11 of 15 individual limestone hand samples (mostly from Taishir, section U1108, Fig. 8C), 2 of 15 partially dolomitized samples (all from section U1111 at Ol Mountain, Fig. 8B) and in 10 of 198 completely dolomitized samples (Figs. 8A, B, D, and 9A-D). $\delta^{13}\text{C}$ values also vary within individual hand samples in the northern Bayan Gorge locality (Fig. 8A) at 188 m in stratigraphic section U1117 and at 143, 219, 227, and 238 m in stratigraphic section U1241 and 1 m in M12016 in Tsakhir Range (Fig. 8D).

The largest isotopic variability in Member T3 of the Taishir Fm is preserved in sample U1108-80 m (Fig. 8G), which is a partially dolomitized carbonate with $\delta^{13}\text{C}$ values ranging between +5.0 to +9.3‰ in a single hand sample. The most positive value is associated with dark grey lime-micrite whereas the values in coarser crystalline textures become lighter. In terms of completely dolomitized T3 carbonate, the most variable values were preserved in sample U1117-106 m (Fig. 8K) sampled in Ol Mountain, where they ranged from +2.7 to +5.5‰. The lowest value is also associated with coarse-crystalline dolostone, which is sugary in texture. This relationship is supported by petrographic observations of dolomitized carbonates (Figs. 7D-F). For instance, the lowest $\delta^{13}\text{C}$ value of +0.7‰, measured in sample U1111-94 m (Fig. 7E), was obtained from medium-coarse crystalline and subhedral dolomite, while the adjacent fine-crystalline, anhedral, and micritic dolomite had a value of +3.1‰. A different view of the same sample is shown in Fig. 7F where only medium-coarse crystalline and subhedral-anhedral dolomite texture is present with a $\delta^{13}\text{C}$ value of +1.8‰. Moreover, petrographic observation of sample U1111-71 m equally revealed two different textures, fine-crystalline anhedral and medium-coarse crystalline subhedral (Fig. 7D), where the lighter $\delta^{13}\text{C}$ value is associated with coarser crystalline texture.

Only two samples of the Ol cap dolostone displayed variability of >2‰. In sample U1112-20.2 m (Fig. 9G), $\delta^{13}\text{C}$ ranged from -2.8 to -0.8‰ and in M12016-1 m, the values ranged from -1.2 to +2.5‰. In these samples, macro-textures do not vary except color distinction between individual laminae. Additionally, a limestone from the upper Ol Fm yielded $\delta^{13}\text{C}$ values that ranged from -4.2 to -1.8‰.

4.3.2. $\delta^{44}\text{Ca}$ and $\delta^{26}\text{Mg}$

Limestone dominated successions: The $\delta^{44/40}\text{Ca}$ values of the basal T3 limestone in the stratigraphic section U1108 covary with the Taishir $\delta^{13}\text{C}$ negative excursion (Figs. 5C and 10B). In the excursion, $\delta^{44/40}\text{Ca}$ values range from -1.7 to -1.3‰. In the rest of the Taishir Fm where very positive $\delta^{13}\text{C}$ values (~+8.5‰) are preserved, limestone $\delta^{44/40}\text{Ca}$ values increase to -1.2‰. Although the $\delta^{44/40}\text{Ca}$ values are not as negative, a similar trend is observed in Uliastai Gorge (F949, Figs. 5F and 10B) in basal T3 limestones where the Taishir negative excursion is expressed. In this section, $\delta^{44/40}\text{Ca}$ values start at -1.2‰, decrease slightly to -1.3‰, and increase to as high as -0.9‰ as the $\delta^{13}\text{C}$ negative excursion returns to positive values. Stratigraphically higher in the same limestone dominated section (F860, Figs. 5C and 10B), lime-micrite of the upper Ol Fm have $\delta^{44/40}\text{Ca}$ values that start at -1.4‰ and increase to -1.1‰ over six meters. Because of the low Mg concentration in limestones, $\delta^{26}\text{Mg}$ was not measured in the limestone successions but $\delta^{26}\text{Mg}$ values were measured in the dolomitized carbonates of the Taishir and Ol fms.

Dolomitized successions: Dolomitized sections of the Taishir Fm measured in northern Bayan Gorge exhibit relatively positive $\delta^{44/40}\text{Ca}$ values compared to Taishir limestone. Particularly, where the basal T3 is dolomitized the $\delta^{44/40}\text{Ca}$ values vary between -1.3‰ to -0.8‰ and display very little variability in the rest of the T3 (~-1.1‰). One sample measured in upper T3 has a value of -1.5‰, which is the

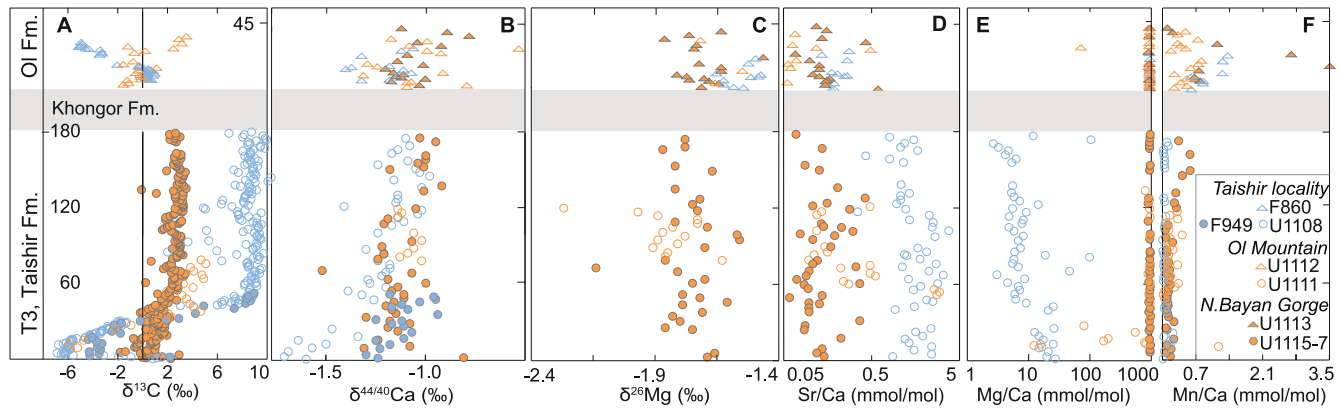


Fig. 10. Co-plots of geochemical data of the Taishir and Ol formations from the Taishir, Ol Mountain, northern Bayan Gorge, and Uliastai Gorge localities. Open and filled blue circles are limestones; and all other symbols are dolomites. A) $\delta^{13}\text{C}$, B) $\delta^{44/40}\text{Ca}$, C) $\delta^{26}\text{Mg}$, D) Sr/Ca (mmol/mol), E) Mg/Ca (mmol/mol), and F) Mn/Ca (mmol/mol). Thickness of the Khongor Formation is not drawn to scale. (For interpretation of the references to color in this figure legend, the reader is referred to the web version of this article.)

lowest value measured in the whole succession.

In the Ol Fm, dolostone of section F860 that overlies the limestones of section U1108 has $\delta^{44/40}\text{Ca}$ values with no apparent correlation to $\delta^{13}\text{C}$ values. In section F860, $\delta^{44/40}\text{Ca}$ values were measured at high resolution (0.5–2.5 m interval) in the Ol cap dolostone and display a trend from $\sim -1.5\text{\textperthousand}$ to $-1.1\text{\textperthousand}$ and correlate with $\delta^{26}\text{Mg}$ values of $-1.5\text{\textperthousand}$. Compared to the cap dolostone section measured in the Taishir locality, the succeeding Ol Fm at northern Bayan Gorge also preserves more positive $\delta^{44/40}\text{Ca}$ values. The $\delta^{44/40}\text{Ca}$ values in the basal cap dolostone are $\sim -1.2\text{\textperthousand}$ to $-1.0\text{\textperthousand}$ and increase to $-0.8\text{\textperthousand}$.

In northern Bayan Gorge (Figs. 5 and 10C), $\delta^{26}\text{Mg}$ values display a uniform profile with an average at $\sim -1.8\text{\textperthousand}$. The values vary from $-2.1\text{\textperthousand}$ to $-1.5\text{\textperthousand}$ and the largest variability is in the dolo-grainstone that directly overlies the dolomitized basal T3 Member. In the Taishir locality (Fig. 5C), the Ol cap dolostone has relatively high $\delta^{26}\text{Mg}$ values with an average of $-1.6\text{\textperthousand}$, ranging from $-1.5\text{\textperthousand}$ to $-1.7\text{\textperthousand}$. Similarly, $\delta^{26}\text{Mg}$ values of the Ol Fm carbonates in Khongor Range (Figs. 6B and 10C) are high with an average at $-1.5\text{\textperthousand}$. The highest value is measured at $-1.2\text{\textperthousand}$ and is present in the Ol cap dolostone. Overall, $\delta^{26}\text{Mg}$ values are more negative in the dolomitized Ol Fm in the northern Bayan Gorge locality and reach values as negative as $-2.1\text{\textperthousand}$.

In the dolomites of the Taishir Fm, there is no apparent covariance between $\delta^{44/40}\text{Ca}$ and $\delta^{13}\text{C}$ values (Figs. 10B and 11A), $\delta^{26}\text{Mg}$ and $\delta^{13}\text{C}$ values (Figs. 10C and 11B), and $\delta^{44/40}\text{Ca}$ and $\delta^{26}\text{Mg}$ values (Fig. 11C). However, in the cap dolostone of the Ol Fm, covariance exists between the $\delta^{13}\text{C}$ and $\delta^{26}\text{Mg}$ values (Fig. 11B) and $\delta^{44/40}\text{Ca}$ and $\delta^{26}\text{Mg}$ values (Fig. 11C) and to a lesser extent $\delta^{44/40}\text{Ca}$ and $\delta^{13}\text{C}$ values.

A total of nine dolomites from the middle Shuurgat Fm at the Khongor Range have $\delta^{44/40}\text{Ca}$ values between $-1.1\text{\textperthousand}$ and $-0.7\text{\textperthousand}$ with an average value at $-1.0\text{\textperthousand}$ (Fig. 6B). Furthermore, $\delta^{26}\text{Mg}$ values in the middle Shuurgat Fm are relatively constant around $\sim -1.8\text{\textperthousand}$ with a minimum at $-1.9\text{\textperthousand}$ and a maximum at $-1.6\text{\textperthousand}$. However, corresponding $\delta^{26}\text{Mg}$ values in Sh4 were more negative and ranged from $-2.4\text{\textperthousand}$ to $-1.9\text{\textperthousand}$ with an average value of $-2.2\text{\textperthousand}$.

4.4. Elemental concentrations

In the Taishir and Ol fms, Mn and Sr concentrations differ between limestone dominated and dolomitized sections (Figs. 10D and F) and stratigraphic patterns are preserved within each measured section. As a whole, the Taishir Fm limestones have relatively high Sr/Ca ratios ($< 3.8 \text{ mmol/mol}$; Fig. 10D). Sr/Ca ratios decrease in the partially dolomitized interval in the middle T3 and increase in the uppermost lime-grainstone and ooid lime-grainstone sequence of T3. In contrast to the limestone, Sr concentrations (Figs. 10D and 11D) are low (Fig. 10E)

and Sr/Ca ratios reach $< 0.6 \text{ mmol/mol}$ (Derry et al., 1992 and references therein) in the dolomitized carbonates of the Taishir Fm (stratigraphic sections measured in Ol Mountain, northern Bayan Gorge, and Tsakhir Range). Sr/Ca ratios in the Ol cap dolostone yield little variability among studied sections, but the lowest numbers are obtained in Ol Mountain and northern Bayan Gorge sections (Fig. 10F). Sr/Ca ratios in the Shuurgat Fm dolostones (Fig. 6B) are low with an average at 0.2 mmol/mol that range from 0.1 and 0.7 mmol/mol.

Mn/Ca ratios of the dolomitized Taishir Fm range between 0.1 and 1.2 mmol/mol, which is much higher than limestones of the Taishir Fm that reach $< 0.2 \text{ mmol/mol}$ (Fig. 10F), with the exception of the basal lime-micrite sequence that preserves the Taishir excursion. Notably, Mn is concentrated more towards the top of the dolomitized Taishir Fm and in the Ol Fm dolomites (Fig. 10F) and Mn/Ca levels in the dolomitized carbonates gradually increase in the uppermost T3. Conversely, Mn/Ca ratios in the Ol cap dolostone measured at Taishir locality are higher than the cap dolostone sequence measured at northern Bayan Gorge locality. Mn/Ca ratios begin at 0.7 mmol/mol and increase to as much as 1.4 mmol/mol. A similar pattern is present in U1113 with concentrations that start at 0.2 mmol/mol and increase to 1.1 mmol/mol with three extremely enriched samples that range from 2.0 to 6.2 mmol/mol. In the rest of the Ol Fm, Mn/Ca averages $\sim 0.2 \text{ mmol/mol}$. Mn/Ca ratios (Fig. 6B) of the Shuurgat Fm dolostone range from 0.1 to 1.9 mmol/mol with an average at 0.3 mmol/mol. The highest concentration is measured in Sh3 and represented by one sample at 1.9 mmol/mol.

4.5. Fluid inclusions

A total of 186 fluid inclusions of the Taishir and Ol fms and an additional 43 from the Keilberg Member were classified as liquid (L) or vapor (V) inclusions based on their phase relationships at room temperature. Three main types of fluid inclusions were recognized under the microscope and their basic features are described below (Fig. S1; Table S3).

Liquid-rich inclusions (type – I) are the most abundant type. They are randomly distributed, colorless, and consist of liquid and vapor phases (two phases, L > V). Their shapes are irregular to rounded and up to 5 μm in length, although most are $< 3 \mu\text{m}$ long (no thermometric data was obtained on fluid inclusions $< 2 \mu\text{m}$ long) and phase ratios by volume % range are from L70-90:V30-10. Liquid inclusions were scattered along seams of calcite or formed clusters of inclusions within carbonate (Figs. S1A–D). Liquid fluid inclusions (type – II) were also abundant. They have regular shapes, but occasionally exhibit necking-down phenomena. Size ranges from several microns to 8 μm . Finally,

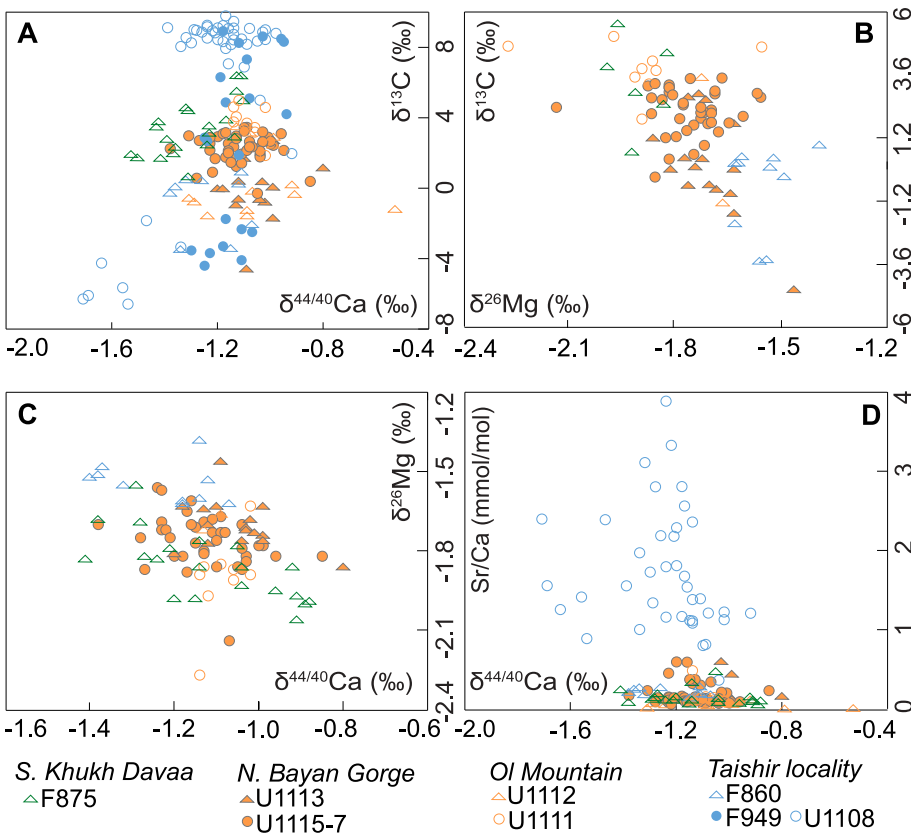


Fig. 11. Cross-plots of geochemical data of the Taishir and Ol formations. Open and filled blue circles are limestones; and all other symbols are dolomites. A) $\delta^{44/40}\text{Ca}$ and $\delta^{13}\text{C}$, B) $\delta^{26}\text{Mg}$ and $\delta^{13}\text{C}$, C) $\delta^{44/40}\text{Ca}$ and $\delta^{26}\text{Mg}$, D) $\delta^{44/40}\text{Ca}$ and Sr/Ca (mmol/mol). (For interpretation of the references to color in this figure legend, the reader is referred to the web version of this article.)

CO_2 inclusions (type – III) (VCO_2) are found in dolostone and limestone samples but are not common. They are relatively regular in shape and black in color. T_h of each phase of type – III inclusions was not measured, as these are difficult to interpret.

T_h in non-dolomitized limestone of the Taishir Fm range from 70 to 194 °C with salinity estimates at 17–29 wt%, which are similar to values preserved in the dolomitized Taishir Fm carbonates (61–187 °C and 5–34 wt% respectively). At the Taishir locality, T_h of the Ol cap dolostone varies between 71 and 148 °C with a salinity of 1–27 wt%, whereas at the Ol Mountain, T_h varies from 69 to 159 °C with a salinity of 21–27 wt%, and at the northern Bayan Gorge, T_h varies from 82 to 151 °C with a salinity of 21–26 wt%. Fluid inclusions of dolomitized upper Ol Fm carbonates at the Ol Mountain and northern Bayan Gorge yielded T_h estimates between 91 and 189 °C with a salinity of 13–29 wt %. Preserved T_h in the Keilberg cap carbonate in Namibia is similarly high, 98–201 °C with salinity at 6–17 wt% (Figs. S1E–F).

5. Discussion

5.1. Litho- and chemostratigraphic features in the Cryogenian-Ediacaran carbonates

The Cryogenian $\delta^{13}\text{C}$ profiles from Namibia (Hoffman, 2011), Arctic Alaska (Macdonald et al., 2009b), and Mongolia (Bold et al., 2016b) preserve significant differences. The Namibian carbonates of the Rasthof, Gruis, Ombaatjie, and Maieberg fms are dominated by dolomite and record three negative $\delta^{13}\text{C}$ excursions, namely the Rasthof excursion ($\delta^{13}\text{C}$ down to $-4\text{\textperthousand}$) in the basal Rasthof Fm, the Trezona excursion ($\delta^{13}\text{C}$ down to $-7\text{\textperthousand}$) in the uppermost Ombaatjie Fm, and the Maieberg excursion in the basal Maeiberg Fm (e.g., Halverson et al., 2005). These negative excursions depart from a positive $\delta^{13}\text{C}$ background value of up to $+6\text{\textperthousand}$ in the Rasthof Fm and up to $+9\text{\textperthousand}$ in the Ombaatjie Fm. The Cryogenian non-glacial interlude of Arctic Alaska is pervasively dolomitized, and preserves the Rasthof excursion, but

stratigraphically higher, values are not as enriched as Namibia and instead hover around $+5\text{\textperthousand}$ with a downturn at the top that could be correlative with the Trezona excursion (Macdonald et al., 2009a). In Mongolia, limestone-dominated strata of the Taishir and Ol fms record the Rasthof and Maieberg excursions along with another negative $\delta^{13}\text{C}$ excursion referred to as the Taishir excursion ($\delta^{13}\text{C}$ down to $-8\text{\textperthousand}$, Fig. 1C), which is interpreted as separate from the Trezona excursion (Bold et al., 2016b).

The initial downturn of the Trezona excursion is potentially preserved at the top of the Taishir Fm, but much of it is absent, perhaps due to sub-glacial erosion (Bold et al., 2016b) or perhaps because the Trezona excursion is a local platform phenomena. Background $\delta^{13}\text{C}$ values from limestone in Mongolia are more isotopically enriched than dolomitized records of Namibia and Arctic Alaska whereas the dolomitized sections are isotopically homogenized and $\delta^{13}\text{C}$ profiles resemble those from Arctic Alaska. Overall, dolomitization appears to dampen Cryogenian $\delta^{13}\text{C}$ fluctuations. Depending on where the stratigraphic sections are measured on the Zavkhan Terrane, variability in $\delta^{13}\text{C}$ between parallel limestone and dolomitized sections is at least 3\textperthousand and can be as much as $12\text{\textperthousand}$, with $\sim 8\text{\textperthousand}$ common.

5.2. Effect of fluid flow on geochemical proxy records

Carbon, Ca, Mg (in case of dolomite), and O are the main elemental components of carbonate rocks and the isotopic signatures of each of these elements can be used to provide constraints on the diagenetic history, the composition of the dolomitizing fluids, and the water–rock ratio. The behavior of these isotopic systems during diagenesis is dependent on the isotopic and elemental concentrations of both the diagenetic fluid and primary sediment. Considering the relatively low concentration of carbon in most diagenetic fluids, the amount of fluid introduced in the Tsagaan-Olom Group must have been high in order for the primary $\delta^{13}\text{C}$ isotopic signatures to be altered in the dolomites. For example, if the dolomitizing fluid was sourced from Ediacaran

seawater, then in order to explain the offset between limestones and dolomites, the C, Ca and Mg isotope compositions of seawater at that time must have either been variable or evolved during dolomitization to explain the offset from the limestones. Furthermore, during dolomitization the fluid itself may have been mixed with groundwater (Wiegand et al., 2015) and consequently changed its isotopic composition along its flow path. Following the approach of Banner and Hanson (1990), Husson et al. (2015) calculated the water-to-rock ratios needed to alter $\delta^{26}\text{Mg}$, $\delta^{44/40}\text{Ca}$, and $\delta^{13}\text{C}$ values of dolomite when the altering fluid is modern seawater. Those authors found that robustness against alteration with modern seawater was favored, in descending order, by $\delta^{13}\text{C}$ to $\delta^{44/40}\text{Ca}$, and to $\delta^{26}\text{Mg}$.

Calcium and Mg isotopes can be used to identify dolomites that have formed during early diagenesis in reaction with seawater (fluid-buffered) in contrast to dolomites formed during later stage alteration (sediment-buffered). Sediments that have been dolomitized in seawater-buffered conditions should have high $\delta^{44/40}\text{Ca}$ values and low $\delta^{26}\text{Mg}$ values and are relatively invariable while sediments that have been dolomitized during sediment-buffered diagenesis should have low $\delta^{44/40}\text{Ca}$ values and variable $\delta^{26}\text{Mg}$ values (Ahm et al., 2018; Higgins et al., 2018). Numerical modeling of early marine dolomitization in Neogene carbonate has shown that it is possible to generate large differences in $\delta^{13}\text{C}$ values (~5‰) during early diagenesis due to differences between fluid- and sediment-buffered conditions (Ahm et al., 2018). This modeling approach allows the fluid composition to evolve during diagenesis, and the extent of open (fluid-buffered) and closed (sediment-buffered) system diagenesis to be tracked with $\delta^{44/40}\text{Ca}$, and to $\delta^{26}\text{Mg}$, which generates predictions for $\delta^{13}\text{C}$, $\delta^{18}\text{O}$, and other chemical systems. This approach was recently used by Ahm et al. (2019), suggesting that the cap dolostones and the observed variability in $\delta^{13}\text{C}$ values were products of early marine dolomitization by seawater during global deglaciation.

In Mongolia, dolomitization appears to have homogenized pre-existing geochemical signatures such as the Taishir negative $\delta^{13}\text{C}$ excursion, its overlying prolonged positive $\delta^{13}\text{C}$ values, and the Maieberg negative $\delta^{13}\text{C}$ excursion in the Ol Fm. The extent of fluid flow or the evolution of the fluid as it reacted with wall-rock along its flow path could explain the differences between individual dolomitized sections. Oxygen isotope values are not significantly different in limestone and dolostone sections suggesting that the $\delta^{18}\text{O}$ of limestones were reset during the dolomitization events or $\delta^{18}\text{O}$ values of both the dolomites and limestones were reset later.

5.2.1. The Taishir Formation

Apart from resetting the $\delta^{13}\text{C}$ signature of the Taishir negative $\delta^{13}\text{C}$ excursion, the covariance between $\delta^{44/40}\text{Ca}$ and $\delta^{13}\text{C}$ (Figs. 5C and 10A-B) profiles is lost in the dolomitized equivalent carbonates in northern Bayan Gorge (Fig. 5A). The same trend is observed in $\delta^{44/40}\text{Ca}$ profile of the same interval in Uliastai Gorge, which coincides with 2‰ difference in $\delta^{13}\text{C}$ compared to that of the Taishir locality section (Fig. 10B). Although these two localities preserve limestone dominated successions of the Taishir Fm, the apparent difference in $\delta^{44/40}\text{Ca}$ and $\delta^{13}\text{C}$ signatures suggests different diagenetic histories. In the rest of the Taishir Fm carbonates (limestone and dolostone), $\delta^{44/40}\text{Ca}$ values are comparable among sections, which may reflect infiltration of dolomitizing fluid in the entire carbonate platform.

5.2.2. The Ol Formation (Marinoan cap carbonate sequence)

During the Marinoan deglaciation, it is hypothesized that anoxic glacial seawater circulated through carbonate platforms, which is supported by the presence of barite overlying cap carbonate sequences worldwide (Ahm et al., 2019; Crockford et al., 2019; Hoffman et al., 2011) including the Ol cap dolostone (Fig. 3F). The circulation of this glacial seawater may have also driven dolomitization and erased the negative $\delta^{13}\text{C}$ excursion that is recorded in limestone of the middle and upper portions of the Ol Fm (Bold et al., 2016b).

The extent to which the dolomitized carbonates of the Taishir and Ol fms formed under excess influence of the dolomitizing fluid (fluid/seawater-buffered condition) or surrounding carbonate (sediment-buffered condition) was assessed using the approach of correlation between $\delta^{44/40}\text{Ca}$ and $\delta^{26}\text{Mg}$ values (Higgins et al., 2018). In the Taishir Fm, both the $\delta^{44/40}\text{Ca}$ and $\delta^{26}\text{Mg}$ values of the dolomitized Taishir Fm carbonates are highly variable, making it difficult to discern the conditions for dolostone formation. However, in the Ol Fm dolostone, covariance exists between $\delta^{44/40}\text{Ca}$ and $\delta^{26}\text{Mg}$ values differ among sections (Figs. 10B-C). $\delta^{26}\text{Mg}$ values become comparatively lower and more variable as dolomitization becomes more pervasive from the Taishir locality to northern Bayan Gorge and further through southern Khukh Davaa. Considering the comparatively lower $\delta^{44/40}\text{Ca}$ values in F860, this trend may track the dominance of fluid-buffered conditions as the entire Ol Fm was dolomitized. Hence, we note that the Taishir and Ol Fm carbonates have a range between fluid and sediment buffered endmembers, depending on the location, and by inference the paleotopography of the platform and dolomitizing fluid pathway.

The Taishir, Ol Mountain and northern Bayan Gorge localities are located along depositional strike with no major facies changes between them (Figs. 2 and 5). Thus, it is difficult to invoke diachronous deposition of the Taishir and Ol Fm carbonates. Based on the observed covariation between $\delta^{44/40}\text{Ca}$, $\delta^{26}\text{Mg}$, and $\delta^{13}\text{C}$ values we suggest that early dolomitization was primarily responsible for dolomitizing the basal Ediacaran cap dolostone of the Ol Fm (Fig. 12). This early dolomitization was more pervasive and extensive than later dolomitizing events and altered the isotopic composition of both the upper Taishir Fm and the basal Ol Fm. Because these formations likely have very different primary compositions, the fluid and sediment-buffered dolomite endmembers of the Taishir and Ol fms record significantly different $\delta^{13}\text{C}$ values. Below (Section 5.4) we use the numerical diagenetic model of Ahm et al. (2018) to test this dolomitization model for the Tsagaan-Olom Group.

We suggest that the apparent variability between limestone and dolostone is in part due to the extreme $\delta^{13}\text{C}$ fluctuations recorded on Neoproterozoic carbonate platforms (Halverson et al., 2010). The range of $\delta^{13}\text{C}$ values are much greater than those in Phanerozoic carbonates (Veizer et al., 1999), although the reason for this difference remains unknown. As a result, dolomitization in Neoproterozoic carbonates may lead to larger changes in the isotopic signature than dolomitization in Phanerozoic carbonates. For example, if the dolomitizing fluid have values that average ~0‰ and alter Phanerozoic rocks that have little isotopic variability to begin with, the effect of dolomitizing on $\delta^{13}\text{C}$ values will be less pronounced.

5.3. Implication of carbonate hosted fluid inclusion in dolomitization

The use of T_h and salinity of fluid inclusions in carbonates are often used to determine the nature of dolomitizing fluids to differentiate dolomitization models, which is based on the assumption that the temperature and composition have not been later reset (Flügel, 2004). However, there are a number of ways to alter fluid inclusion data from carbonates (heterogeneous entrapment, necking down process, and thermal re-equilibration etc., Bodnar, 2003; Burruss, 1987; Goldstein, 1993, 2001; Lacazette, 1990). Shape-wise, all of the fluid inclusions measured in this study are compatible with a primary origin; however, extremely high temperatures from some samples suggest resetting during burial (Section 4.5).

In general, T_h of < 50 °C and salinity between fresh water and seawater are assumed to be representative of mixing-zone environment whereas T_h between 82 °C and > 165 °C and salinity between 12 wt% and 28 wt% (NaCl eq.) are characteristic of dolomites formed in hydrothermal environment (Braithwaite and Rizzi, 1997; Luczaj, 2006), or through brine reflux (Emsbo, 2017; Polito et al., 2006). In the studied carbonates of both Mongolia and Namibia, the T_h estimates are comparable and reach < 200 °C (Fig. S1E) and the salinity constraints are

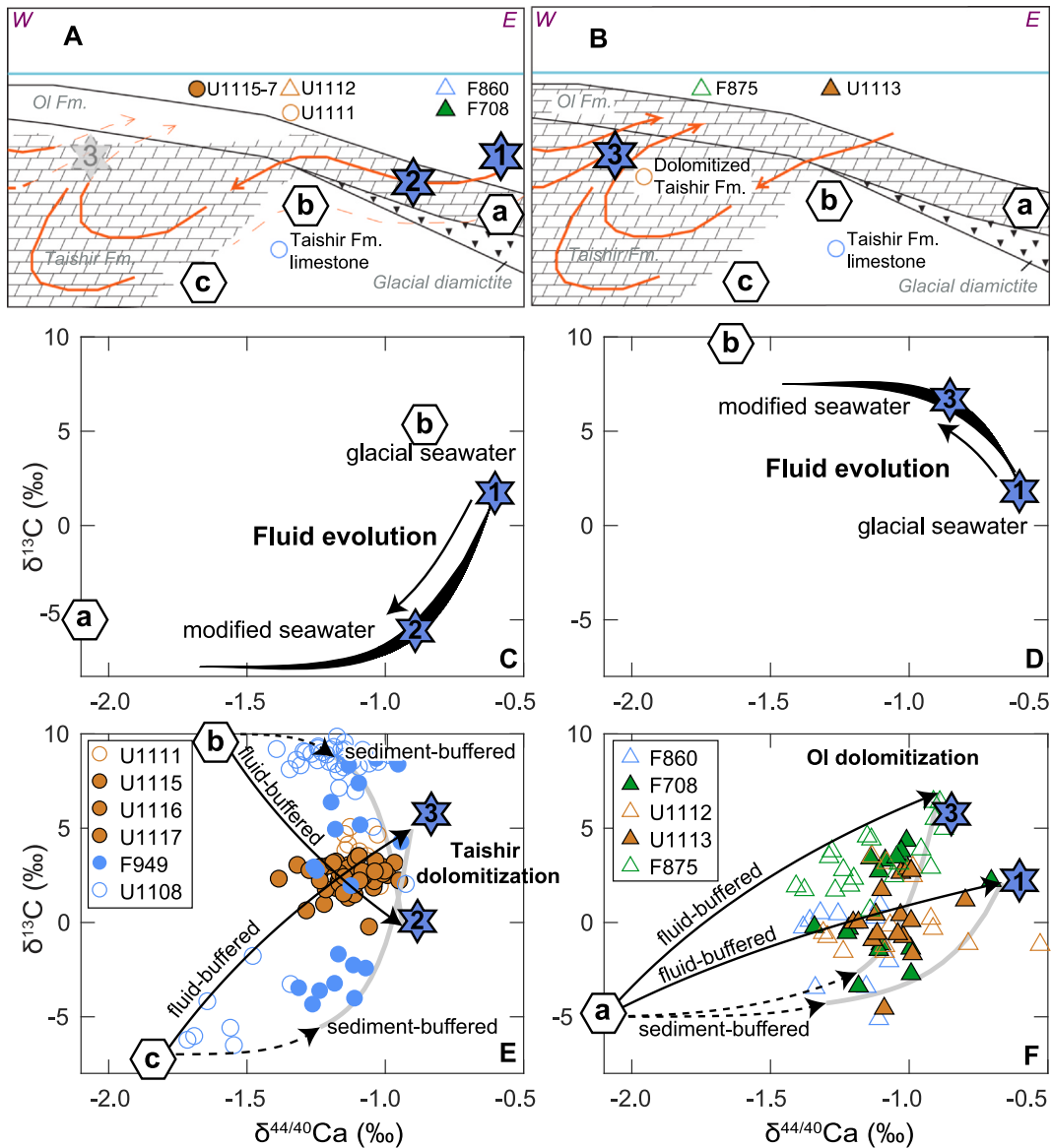


Fig. 12. Modeled sequence for dolomitization by early marine diagenesis in Dolomitization event 1. For numerical values, refer to Table 1. In A and B, orange arrows reflect fluid flow pathway and letters a, b, and c refer to points on the geochemical evolution of dolomitizing fluids shown in C, D, E, and F. A) Initial infiltration of dolomitizing fluid (glacial deep marine seawater (1)) into the down-dip section of the platform. Geochemical evolution within the Ol Formation shown by blue star (2). The Khongor Formation shale acts as a seal and restricts dolomitization. Farther up dip, dolomitizing fluid travels into the upper Taishir Formation, whose primary geochemical signature is different than the Ol Formation, thus the fluid further evolves to grey star (3). B) In each up-dip locality, chemical composition of dolomitizing fluid differs. Glacial seawater enters the Ol carbonates and flows into the Taishir Formation where it is modified, producing a new fluid enriched in $\delta^{13}\text{C}$ denoted by blue star (3). This new fluid starts to ascend and infiltrates through the Ol Formation carbonates resulting in especially high $\delta^{13}\text{C}$ values in the dolomitized Ol cap dolostone (F875). C) Fluid evolution from the reaction between glacial seawater (1, Table 1) and Marinoan cap carbonate (a – the basal Ol Formation) resulting in low $\delta^{13}\text{C}$ values. D) Fluid evolution from the reaction between glacial seawater (1) and Taishir limestone with high $\delta^{13}\text{C}$ (b) to produce a modified seawater (3). E) Bulk sediment $\delta^{13}\text{C}$ and $\delta^{44/40}\text{Ca}$ values during multistage Taishir Formation dolomitization. First, the Taishir limestone with high $\delta^{13}\text{C}$ (b) reacts along a fluid-buffered pathway with the modified fluid (2). Second, the Taishir limestone with light $\delta^{13}\text{C}$ (c) reacts with the modified high fluid (3) along a sediment buffered pathway. F) Bulk sediment evolution of $\delta^{13}\text{C}$ and $\delta^{44/40}\text{Ca}$ values during multistage Ol Formation dolomitization. First, the Marinoan cap carbonate (a – basal Ol Formation) reacts with glacial seawater (1) along a fluid buffered pathway. Second, the Marinoan cap carbonate (a) reacts with the modified high fluid (3) along pathways ranging from fluid to sediment buffered. (For interpretation of the references to color in this figure legend, the reader is referred to the web version of this article.)

high, > 12 wt% (NaCl eq., Fig. S1F) on average, which favor either hydrothermal or brine reflux dolomitization regime. However, burial temperatures associated with Ediacaran to Paleozoic orogenies in both Mongolia and Namibia, and burial from overlying strata that are no longer preserved, may account for high fluid inclusion temperatures. Hence, taking into account the low susceptibility of salinity resetting in aqueous inclusions during metamorphism (Burruss, 1987; Osborne and Haszeldine, 1993), we only cite salinity constraints in our

dolomitization model. Considering the fact that salinity estimates are even higher in Mongolia than Namibian carbonates, we may expect even larger input from brine reflux or basinal fluids in dolomitization. This suggests that dolomitizing fluids are different in these regions due to varying geologic setting with different burial histories. With the existing fluid inclusion dataset, it is not possible to constrain variability recorded along a dolomitizing fluid flow path.

5.4. Dolomitization model

To explain the large variations in geochemical proxies, the dolomitizing fluid and permeability structure (Nogues et al., 2013) of the Mongolian carbonates were likely effected in at least two major stages (Fig. 12). First, stratigraphic and geochemical data demonstrate that Dolomitization Event 1 occurred before full lithification of the basal Ol and uppermost Taishir Fm carbonates. Second, textural data (saddle dolomites and destruction of depositional textures etc. in the Taishir carbonates) require a later/subsequent dolomitization event, Dolomitization Event 2, responsible for dolomitizing the Shuurgat Fm.

The first stage of dolomitization during early burial (i.e. within meters to tens of meters of the sediment water-interface) is favored for the lower Tsagan-Olom Group for three reasons. First, this environment can easily provide a sufficient supply of Mg for dolomitization due to circulation of seawater. Second, the covariance between $\delta^{26}\text{Mg}$ and $\delta^{44/40}\text{Ca}$ values are similar to those from other cap dolostone successions from across the globe (Ahm et al., 2019). This dolomitization event associated with termination of the last Snowball Earth is hypothesized to be associated with the recirculation of seawater mixed with glacial meltwater (Figs. 12A-B). In this scenario, cold, saline seawater travels deep into the carbonate platform, and expels upwards as meltwater discharge from land. In addition, the depositional model of Bold et al. (2016a) for the Tsagan-Olom Group suggests that a topographic high was created during the deposition of the upper Taishir Fm, which may have facilitated localized movement of groundwater in porous carbonate textures. Lithologically and texturally, early to syn-depositional dolomitization is consistent with the absence of evaporites in the Taishir and Ol fms and a presence of fabric retentive dolostone textures.

Third, salinity estimates recorded in fluid inclusions of the dolomitized carbonates (including the Keilberg carbonate of Namibia) are elevated (> 12 wt% on average), which is consistent with glacial brines that form beneath ice sheets. Yang et al. (2017) estimated a salinity of $\sim 7\%$ in Snowball brines, twice as high as modern seawater. Additional salinity may have been provided by the expulsion of basinal brines by both unloading an ~ 2 km thick ice sheet, but also via a deep basinal flow path of the cold saline seawater brine. In absence of evidence of evaporites on the Zavkhan terrane, the highest salinity values from Mongolian samples (> 20 wt%) imply local input of deeply buried fluid, which is supported by enrichment of Mn in dolomitized successions (Fig. 10F). After careful screening of our geologic data, we propose the following sequences for dolomitization.

5.4.1. Dolomitization event 1

Dolomitization of the Ol cap carbonates: In the Taishir locality and Khongor Range, only the Ol cap dolostone is dolomitized, whereas the underlying Taishir Fm and overlying rest of the Ol Fm carbonates are preserved as limestone. We propose that during Marinoan deglaciation, when dolomitizing fluids initiated their first path into the Zavkhan platform (Fig. 12A; Table 1), the basal Ol Fm was preferentially dolomitized. At that time, the Khongor Fm shale between the Ol and Taishir carbonates was regionally an impermeable boundary to diagenetic

fluid, but locally that barrier was ineffective as evidenced by rare beds of partially dolomitized carbonate in the upper Taishir at locations such as the Taishir locality (Fig. 8C) due to the variable thickness of the shale from 0 to 25 m.

Geochemical variability recorded within these Ol cap dolostone successions can be explained (Figs. 12A, C, and F) by fluid- to sediment-buffered dolomitization in glacial deep seawater. Fluid-buffered early marine dolomitization is characterized by high $\delta^{44/40}\text{Ca}$ values ($-0.8\text{\textperthousand}$) and low $\delta^{26}\text{Mg}$ values ($-1.85\text{\textperthousand}$) whereas sediment-buffered dolomitization is characterized by low $\delta^{44/40}\text{Ca}$ ($\sim -1.4\text{\textperthousand}$) values and high $\delta^{26}\text{Mg}$ values ($\sim -1.4\text{\textperthousand}$). Based on our carbonate hosted fluid inclusion salinity estimate, the modified seawater salinity at that time appears to have been high, > 12 wt%.

As a test of our hypothesis above, we use a diagenetic model (Ahm et al., 2018) to estimate the evolution of the dolomitizing fluid along the flow path. The composition of the initial dolomitizing fluid is set to Marinoan seawater, previously estimated from multiple cap carbonate sequences (Table 1; Ahm et al., 2019). The composition of the initial dolomitizing fluid evolves along the flow path in reaction with previously deposited carbonate sediments (Figs. 12C and F). For example, at the Taishir locality where glacial seawater locally circulated through the upper Taishir Fm limestones, the dolomitizing fluid evolved towards higher $\delta^{13}\text{C}$ values (Figs. 12A and D; Table 1). Following reaction with the Taishir Fm limestones, the dolomitizing fluid then penetrated the Ol cap dolostone of northern Bayan Gorge (U1113) where geochemical variability is even larger and becomes more positive (Fig. 9B). To explain these high $\delta^{13}\text{C}$ values at northern Bayan Gorge, we must invoke geochemical evolution of the dolomitizing fluid from reaction with the upper Taishir Fm limestones with high $\delta^{13}\text{C}$ values (+8 to +9‰) (Figs. 12A, C, and F, modified fluid 2, Table 1). As a result, the geochemical variability in each locality in the Zavkhan Terrane can be explained by evolution of the dolomitizing fluid due to reactions with the sediment along its flow path.

Dolomitization of the upper Taishir Fm: To the west from the Taishir locality (Figs. 2A, 5B, and 8B), dolomitization of the upper Taishir Fm carbonates becomes pervasive and expansive. The increase in pervasive dolomitization coincides with a decrease in the thickness of the overlying Khongor Fm shale and a more homogenized geochemical signature in the underlying Taishir Fm. Specifically, the very positive $\delta^{13}\text{C}$ values of the limestone precursors (upper Taishir Fm) become less positive and the very negative values (Taishir and Maeiberg negative excursions) become less negative (Figs. 5, 8, and 9). This decrease in variability is also consistent with a dolomitizing fluid that was modified to lower $\delta^{13}\text{C}$ values by reaction with the precursor Marinoan cap carbonate it infiltrated through before reaching with the upper Taishir Fm carbonates (Fig. 12A; Table 1). In this dolomitization sequence, results from the diagenetic model suggest that the dolomitizing fluid evolved from the initial composition of glacial seawater towards a modified composition (fluid 2 – Table 1) with a $\delta^{13}\text{C}$ value of $-6.1\text{\textperthousand}$, $\delta^{44/40}\text{Ca}$ of $-0.9\text{\textperthousand}$, and $\delta^{26}\text{Mg}$ of $0.1\text{\textperthousand}$ due to reaction with the host carbonate with a $\delta^{13}\text{C}$ value of $\sim +10\text{\textperthousand}$, $\delta^{44/40}\text{Ca}$ of $-1.7\text{\textperthousand}$, and $\delta^{26}\text{Mg}$ of $-2.1\text{\textperthousand}$ (Fig. 12C).

Dolomitization of the basal Ediacaran cap carbonate: In our model,

Table 1
Numeric model parameters for the modeled sequence for Dolomitization event 1.

	$\delta^{44/40}\text{Ca}$ (‰)	$\delta^{26}\text{Mg}$ (‰)	$\delta^{13}\text{C}$ (‰)	Description
<i>Fluid</i>				
Glacial deep seawater (1)	-0.6	-0.2	2.0	Glacial seawater model estimates from Ahm et al. (2019)
Modified fluid (2)	-0.9	0.1	-6.1	Modified seawater, evolved by reaction with the Ol cap carbonate
Modified fluid (3)	-0.9	0.1	6.5	Modified seawater, evolved by reaction with the Taishir Fm. Heavy $\delta^{13}\text{C}$ (‰) limestones
<i>Solid</i>				
Ol Cap carbonate (a)	-2.1	-1.0	-5.0	Primary composition of the cap carbonate, estimated by Ahm et al. (2019)
Taishir Fm. heavy $\delta^{13}\text{C}$ (‰) limestone (b)	-1.7	-1.0	10.0	Primary sedimentary values of the upper Taishir Fm. limestones
Taishir Fm. Negative $\delta^{13}\text{C}$ (‰) nadir (c)	-1.7	-1.0	-7.0	Primary sedimentary values of the Taishir negative $\delta^{13}\text{C}$ (‰) excursion limestones

evolution of dolomitizing fluid plays an important role in explaining the geochemical variability. In fact, the high $\delta^{13}\text{C}$ value of $\sim +7.3\text{\textperthousand}$ recorded in the Ol cap dolostone (F875, Fig. 5E) requires that the dolomitizing fluid had exceptionally high $\delta^{13}\text{C}$ values which is consistent with a modified fluid (3) portraying the primary geochemical signature of the upper Taishir Fm limestone (Figs. 12B, D and F; Table 1). The diagenetic numerical model estimates a dolomitizing fluid (fluid 3 – Table 1) with $\delta^{13}\text{C}$ value of $+6.5\text{\textperthousand}$, $\delta^{44/40}\text{Ca}$ of $-0.9\text{\textperthousand}$, and $\delta^{26}\text{Mg}$ of $0.1\text{\textperthousand}$ that was modified by reactions with the Ol cap carbonate with an initial composition set at $\delta^{13}\text{C}$ value of $-5\text{\textperthousand}$, $\delta^{44/40}\text{Ca}$ of $-2.1\text{\textperthousand}$, and $\delta^{26}\text{Mg}$ of $-1\text{\textperthousand}$.

5.4.2. Dolomitization event 2

Dolomitization of the Shuurgat Fm: Fabric destructive textures in the Shuurgat Fm suggest a subsequent dolomitization event associated with fluid flow during deeper burial. This latter dolomitization may have been more expansive and resulted in an almost complete dolomitization of the entire Shuurgat Fm except the limited preservation of limestone strata in the Sh3-4. There is some geochemical variability ($\delta^{13}\text{C}$ variability of $\sim 4\text{\textperthousand}$) preserved between the co-existing limestone and dolomitized carbonates (Fig. 6; Bold et al., 2016b).

Fabric destructive dolomitization often results from circulation of dolomitizing fluid after lithification and may have occurred either during or before foreland basin development (545–525 Ma, Fig. S2) on the Zavkhan Terrane (Smith et al., 2016). Metamorphism and subduction related magmatism in the hinterland between 579 and 537 Ma (Demoux et al., 2009; Jian et al., 2014) provide evidence for middle Ediacaran orogenesis to the southwest of the terrane, which could have provided the topography to drive fluid flow and burial dolomitization. In the foreland diagenetic zone, orogenesis can trigger carbonate dissolution, dolomitization, and porosity generation in carbonate successions (Heydari, 1997). Due to an increased geothermal gradient and nearby heat source from magmatism, hot and saline fluids can migrate upwards through faults (Davies and Smith, 2006) and laterally through permeable units. An analogous setting has been proposed for dolomitization of the Cambro-Ordovician platform in the Canadian Appalachians where Early to Middle Ordovician accretionary events drove hot saline fluids along faults and through the platform prior to deposition in the Middle to Late Ordovician foreland basin (Lavoie and Chi, 2010).

5.5. Implications for the Neoproterozoic seawater composition

As demonstrated in the Neogene of the Bahamas and southwest Australia, the geochemical composition ($\delta^{13}\text{C}$, $\delta^{26}\text{Mg}$, and $\delta^{44/40}\text{Ca}$) of platform top carbonates can differ significantly from seawater due to primary mineralogy, early marine diagenesis, and local DIC sources (Higgins et al., 2018; Swart, 2008; Swart and Eberli, 2005). Nonetheless, broadly synchronous $\delta^{13}\text{C}$ changes have been recorded in four modern platforms worldwide, Bahamas, Maldives, Queensland plateau, and Great Australian Bight, but significantly different changes are recorded in peri-platform and deep sea pelagic carbonates (Swart, 2008). The coincidence with sea-level change points to a common early diagenetic origin for the geochemical variability observe in shallow-water carbonates (Higgins et al., 2018). Moreover, on modern platforms it is often the dolomites which have experienced the highest degree of open system early diagenesis that preserve $\delta^{13}\text{C}$ values that are closest to modern seawater.

In contrast to observations from modern platform dolomites, we do not know the Neoproterozoic diagenetic conditions and have few constraints on the $\delta^{13}\text{C}$ value of past seawater. However, the Neoproterozoic composite $\delta^{13}\text{C}$ curve is composed of platform top carbonates which are unlikely to record the $\delta^{13}\text{C}$ values of open ocean seawater. Although the $\delta^{13}\text{C}$ of organic and carbonate carbon isotopes covary through the Taishir Fm with $\sim 20\text{\textperthousand}$ variation (Johnston et al., 2012), this only demonstrates that carbonates faithfully record the primary local

dissolved inorganic carbon values, but does not guarantee that these are open ocean seawater values (Oehlert and Swart, 2014). Strontium isotope values through the Taishir Fm also appear to be consistent with seawater (Bold et al., 2016b), but strontium has a longer residence time than carbon in the ocean and is less sensitive to local changes in productivity and restriction across the platform. Importantly, in both the Taishir and Ol fms, dolostones characterized by early fluid-buffered diagenesis have very different isotopic values from limestones. The fact that you can see this variability not only in Cryogenian carbonates in Mongolia, but also in the Yukon (Macdonald et al., 2018), Arctic Alaska (Macdonald et al., 2009b), NW Canada, and Namibia, suggests that something peculiar was happening in Cryogenian platforms environments that affected the $\delta^{13}\text{C}$ composition of platform-top carbonates relative to open ocean seawater (Ahm et al., 2019; Husson et al., 2015).

On the Zavkhan platform, the major dolomitization event is interpreted to have taken place in the early marine diagenetic realm by a diagenetic fluid that is derived mainly from Marinoan glacial seawater (Section 5.4). The isotopic variability of $\delta^{44/40}\text{Ca}$, $\delta^{26}\text{Mg}$, and $\delta^{13}\text{C}$ in the dolostones is consistent with alteration in Marinoan glacial seawater, which implies that the fluid-buffered dolomitized Tsagaan-Olom Group carbonates more accurately recorded the open ocean seawater composition than the stratigraphically equivalent limestone strata. However, the composition of this fluid was clearly modified during its flow-path, which complicates precise assessments of the $\delta^{13}\text{C}$ value of Neoproterozoic seawater. Moreover, although it is tempting to suggest that Neoproterozoic dolomites may be a better recorder of seawater because they have likely seen more fluid-buffered diagenesis, but our study demonstrates that these dolomites can have a complicated history.

Although we do not have an explanation for the ultimate drivers of the anomalously enriched and depleted $\delta^{13}\text{C}$ values on Cryogenian platform tops, or a revision to the Neoproterozoic seawater curve, we emphasize that isolating the geochemistry of the platform from that of seawater and diagenetic waters does not diminishes the value of Neoproterozoic $\delta^{13}\text{C}$ carbonate studies. In fact, it provides a way to reconcile conflicts between organic carbon burial (f_{org}) interpretations of the carbon cycle, large apparent changes in $\delta^{13}\text{C}$ values from platform carbonate values, and paleo-redox data.

6. Conclusion

The Neoproterozoic Tsagaan-Olom Group of Mongolia hosts co-existing limestone and dolostone successions that span the late Cryogenian and earliest Ediacaran period. The $\delta^{13}\text{C}$ values of the dolomitized strata vary significantly from limestone strata. Along strike, variability of $3\text{--}12\text{\textperthousand}$ in $\delta^{13}\text{C}$ is preserved between limestone-dominated and dolomitized carbonate successions of the Taishir and Ol fms. The Ol cap dolostone is always preserved as dolostone; however, variable $\delta^{13}\text{C}$ values are preserved where the Ol cap dolostone is bound by limestone, versus where both underlying Taishir and rest of the Ol Fm carbonates are affected by dolomitization. Map relationships, petrography, geochemistry, and fluid inclusions suggest that dolomitization of the upper Taishir and Ol fm carbonates occurred in a shallow water early diagenetic environment via mixing of glacial meltwater and seawater. Using a numerical modeling approach, the evolution of the dolomitizing fluid and its effect on the geochemical composition of the Tsagaan-Olom Group carbonates are characterized. Early marine dolomitization, Dolomitization Event 1, occurred during deposition of the Ol cap dolostone, and the composition of the fluid evolved as it dolomitized the upper Taishir Fm carbonates and the Ol Fm. Dolomitization of the Shuurgat Fm occurred later, Dolomitization Event 2, and can be related to latest Ediacaran to early Cambrian orogenic fluids. Extremely high $\delta^{13}\text{C}$ values and large negative excursions in shallow water limestone of the Tsagaan-Olom Group become muted in dolomitized sections. As the dolomitizing fluids were derived from seawater, albeit modified along their flow path, their fluid buffered $\delta^{13}\text{C}$ values are

likely closer to original seawater values. The origin and significance of extreme $\delta^{13}\text{C}$ values on Neoproterozoic platforms remains an enigma, but lateral differences in $\delta^{13}\text{C}$ between dolomitized sections or localities are most easily produced by early diagenesis rather than isotopic gradients in seawater.

Declaration of Competing Interest

The authors declare that they have no known competing financial interests or personal relationships that could have appeared to influence the work reported in this paper.

Acknowledgements

We would like to thank the MIT node of the NASA Astrobiology Institute and NASA Astrobiology grant NNH10ZDA001N-EXO for support. ASCA acknowledges support from the Carlsberg Foundation and the Simons Foundation (grant no. 611878). We would also like to thank Greg Eischeid and Sarah Manley for help in the laboratory to collect carbon and oxygen isotopes and clumped isotope paleothermometry data; Elizabeth Lundstrom for help in the laboratory to collect elemental concentration data; Paul Hoffman for providing samples of the Keilberg cap dolostone for fluid inclusion studies. Ogata Takeyuki of Department of Earth Resource Science of Akita University for useful comments and help in the laboratory. We also thank David Budd for constructive comments and edits to make the flow of scientific content as clear and understandable as possible.

Appendix A. Supplementary data

Supplementary data to this article can be found online at <https://doi.org/10.1016/j.precamres.2020.105902>.

References

- Ahm, A.-S., Bjerrum, C.J., Blättler, C.L., Swart, P.K., Higgins, J.A., 2018. Quantifying early marine diagenesis in shallow-water carbonate sediments. *Geochim. Cosmochim. Acta* 236, 140–159.
- Ahm, A.-S., Maloof, A.C., Macdonald, F.A., Hoffman, P.F., Bjerrum, C.J., Bold, U., Rose, C.V., Strauss, J.V., Higgins, J.A., 2019. An early diagenetic deglacial origin for basal Ediacaran “cap dolostones”. *Earth Planet. Sci. Lett.* 506, 292–307.
- Antonellini, M., 2000. A natural analog for a fractured and faulted reservoir in dolomite: triassic Sella Group, northern Italy. *AAPG Bull.* 84 (3), 314–344.
- Arvidson, R.S., Mackenzie, F.T., 1999. The dolomite problem: control of precipitation kinetics by temperature and saturation state. *Am. J. Sci.* 299 (4), 257–288.
- Banner, J.L., Hanson, G.N., 1990. Calculation of simultaneous isotopic and trace element variations during water-rock interaction with application to carbonate diagenesis. *Geochim. Cosmochim. Acta* 54, 3123–3137.
- Blättler, C.L., Miller, N.R., Higgins, J.A., 2015. Mg and Ca isotope signatures of authigenic dolomite in siliceous deep-sea sediments. *Earth Planet. Sci. Lett.* 419, 32–42.
- Blount, D.N., Moore Jr, C.H., 1969. Depositional and non-depositional carbonate breccias, Chiantla Quadrangle, Guatemala. *Geol. Soc. Am. Bull.* 80 (3), 429–442.
- Bodnar, R.J., 1993. Revised equation and table for determining the freezing point depression of H₂O-NaCl solutions. *Geochim. Cosmochim. Acta* 57 (3), 683–684.
- Bodnar, R.J., 2003. Reequilibration of fluid inclusions. In: *Fluid Inclusions: Analysis and Interpretation*, pp. 213–230.
- Bold, U., Crowley, J.L., Smith, E.F., Sambuu, O., Macdonald, F.A., 2016a. Neoproterozoic to early Paleozoic tectonic evolution of the Zavkhan Terrane of Mongolia: Implications for crustal growth in the Central Asian Orogenic Belt. *Lithosphere* 8 (6), 729–750.
- Bold, U., Smith, E.F., Rooney, A.D., Buchwaldt, R., Ramezani, J., Schrag, D.P., Macdonald, F.A., 2016b. Neoproterozoic stratigraphy of the Zavkhan Terrane of Mongolia: the backbone for Cryogenian and Early Ediacaran chemistratigraphic records. *Am. J. Sci.* 316, 1–63.
- Braithwaite, C., Rizzi, G., 1997. The geometry and petrogenesis of hydrothermal dolomites at Navan, Ireland. *Sedimentology* 44 (3), 421–440.
- Brand, U., 2004. Carbon, oxygen and strontium isotopes in Paleozoic carbonate components: an evaluation of original seawater-chemistry proxies. *Chem. Geol.* 204 (1), 23–44.
- Burruss, R.C., 1987. Diagenetic palaeotemperatures from aqueous fluid inclusions: re-equilibration of inclusions in carbonate cements by burial heating. *Mineral. Mag.* 51 (62), 477–481.
- Crockford, P.W., Wing, B.A., Paytan, A., Hodgskiss, M.S.W., Mayfield, K.K., Hayles, J.A., Middleton, J.E., Ahm, A.-S., Johnston, D.T., Caxito, F., Uhlein, G., Halverson, G.P., Eickmann, B., Torres, M., Horner, T.J., 2019. Barium-isotopic constraints on the origin of post-Marinoan barites. *Earth Planet. Sci. Lett.* 519, 234–244.
- Davies, G.R., Smith Jr, L.B., 2006. Structurally controlled hydrothermal dolomite reservoir facies: an overview. *Bulletin* 90 (11), 1641–1690.
- Degens, E.T., Epstein, S., 1964. Oxygen and carbon isotope ratios in coexisting calcrites and dolomites from recent and ancient sediments. *Geochim. Cosmochim. Acta* 28 (1), 23–44.
- Demoux, A., Kröner, A., Badarch, G., Jian, P., Tomurhuu, D., Wingate, M.D., 2009. Zircon Ages from the Baydrag Block and the Bayankhongor Ophiolite Zone: time constraints on late Neoproterozoic to Cambrian subduction- and accretion-related magmatism in Central Mongolia. *J. Geol.* 117 (4), 377–397.
- Derry, L.A., Kaufman, A.J., Jacobsen, S.B., 1992. Sedimentary cycling and environmental change in the Late Proterozoic: evidence from stable and radiogenic isotopes. *Geochim. Cosmochim. Acta* 56, 1317–1329.
- Diehl, S., Hofstra, A., Koenig, A., Emsbo, P., Christiansen, W., Johnson, C., 2010. Hydrothermal zebra dolomite in the Great Basin, Nevada—attributes and relation to Paleozoic stratigraphy, tectonics, and ore deposits. *Geosphere* 6 (5), 663–690.
- Emsbo, P., 2017. Sedex brine expulsions to Paleozoic basins may have changed global marine 87Sr/86Sr values, triggered anoxia, and initiated mass extinctions. *Ore Geol. Rev.*
- Evamy, B., 1963. The application of a chemical staining technique to a study of dedolomitisation. *Sedimentology* 2 (2), 164–170.
- Fantle, M.S., DePaolo, D.J., 2007. Ca isotopes in carbonate sediment and pore fluid from ODP Site 807A: the Ca₂₊(aq)-calcite equilibrium fractionation factor and calcite recrystallization rates in Pleistocene sediments. *Geochim. Cosmochim. Acta* 71 (10), 2524–2546.
- Fantle, M.S., Higgins, J., 2014. The effects of diagenesis and dolomitization on Ca and Mg isotopes in marine platform carbonates: implications for the geochemical cycles of Ca and Mg. *Geochim. Cosmochim. Acta* 142, 458–481.
- Flügel, E., 2004. *Microfacies of Carbonate Rocks: Analysis, Interpretation and Application*. Springer, Berlin, pp. 976.
- Folk, R., 1965. *Petrology of Sedimentary Rocks (PDF Version)*, second ed. Hemphill's Bookstore, Austin ISBN 0-914696-14-9.
- Goldstein, R.H., 1993. Fluid inclusions as carbonate microfabrics: a petrographic method to determine diagenetic history. In: *Carbonate Microfabrics*. Springer, pp. 279–290.
- Goldstein, R.H., 2001. Fluid inclusions in sedimentary and diagenetic systems. *Lithos* 55 (1), 159–193.
- Grotzinger, J.P., Knoll, A.H., 1995. Anomalous carbonate precipitates: is the Precambrian the key to the Permian? *Palaeos* 10 (6), 578–596.
- Gussone, N., Böhm, F., Eisenhauer, A., Dietzel, M., Heuser, A., Teichert, B.M.A., Reitner, J., Wörheide, G., Dullo, W.-C., 2005. Calcium isotope fractionation in calcite and aragonite. *Geochimica et Cosmochimica Acta* 69 (18), 4485–4494.
- Gussone, N., Ahm, A.-S., Lau, K.V., Bradbury, H.J., 2020. Calcium isotopes in deep time: potential and limitations. *Chem. Geol.* 119601.
- Halverson, G.P., 2006. A Neoproterozoic chronology. In: Xiao, S., Kaufman, A.J. (Eds.), *Neoproterozoic Geobiology and Paleobiology*. Springer, New York, NY, pp. 231–271.
- Halverson, G.P., Hoffman, P.F., Schrag, D.P., Kaufman, A.J., 2002. A major perturbation of the carbon cycle before the Ghuab glaciation (Neoproterozoic) in Namibia: Prelude to snowball Earth?: major perturbation of the carbon cycle. *Geochem.-Geophys.-Geosyst.* 3 (6). <https://doi.org/10.1029/2001GC000244>.
- Halverson, G.P., Maloof, A.C., Hoffman, P.F., 2004. The Marinoan glaciation (Neoproterozoic) in northeast Svalbard: Basin Rese. 16, 297–324.
- Halverson, G.P., Hoffman, P.F., Schrag, D.P., Maloof, A.C., Rice, A.H.N., 2005. Toward a Neoproterozoic composite carbon-isotope record. *Geol. Soc. Am. Bull.* 117 (9–10), 1181–1207.
- Halverson, G.P., Wade, B.P., Hurtgen, M.T., Barovich, K.M., 2010. Neoproterozoic che-mostratigraphy. *Precambrian Res.* 182 (4), 337–350.
- Heydari, E., 1997. Hydrotectonic models of burial diagenesis in platform carbonates based on formation water geochemistry in North American sedimentary basins.
- Higgins, J.A., Schrag, D.P., 2010. Constraining magnesium cycling in marine sediments using magnesium isotopes. *Geochim. Cosmochim. Acta* 74 (17), 5039–5053.
- Higgins, J.A., Blättler, C.L., Lundstrom, E.A., Santiago-Ramos, D.P., Akhtar, A.A., Crüger Ahm, A.-S., Bialik, O., Holmden, C., Bradbury, H., Murray, S.T., Swart, P.K., 2018. Mineralogy, early marine diagenesis, and the chemistry of shallow-water carbonate sediments. *Geochim. Cosmochim. Acta* 220, 512–534.
- Hoffman, P.F., 2011. Strange bedfellows: glacial diamictite and cap carbonate from the Marinoan (635 Ma) glaciation in Namibia. *Sedimentology* 58, 57–119.
- Hoffman, P.F., Macdonald, F.A., Halverson, G.P., 2011. Chemical sediments associated with Neoproterozoic glaciation: iron formation, cap carbonate, barite and phosphorite. In: Arnaud, E., Halverson, G.P., Shields, G. (Eds.), *The Geologic Record of Neoproterozoic Glaciations*. London: Geological Society of London.
- Husson, J.M., Higgins, J.A., Maloof, A.C., Schoene, B., 2015. Ca and Mg isotope constraints on the origin of Earth's deepest 813C excursion. *Geochim. Cosmochim. Acta* 160, 243–266.
- Jacobson, A.D., Holmden, C., 2008. 844Ca evolution in a carbonate aquifer and its bearing on the equilibrium isotope fractionation factor for calcite. *Earth Planet. Sci. Lett.* 270 (3), 349–353.
- Jahn, B.M., Litvinovsky, B.A., Zanvilevich, A.N., Reichow, M., 2009. Peralkaline granitoid magmatism in the Mongolian-Transbaikalian Belt: evolution, petrogenesis and tectonic significance. *Lithos* 113, 521–539.
- Jian, P., Kröner, A., Jahn, B.-M., Windley, B.F., Shi, Y., Zhang, W., Zhang, F., Miao, L., Tomurhuu, D., Liu, D., 2014a. Zircon dating of Neoproterozoic and Cambrian ophiolites in West Mongolia and implications for the timing of orogenic processes in the central part of the Central Asian Orogenic Belt. *Earth Sci. Rev.* 133, 62–93.
- Jiang, G., Kaufman, A.J., Christie-Blick, N., Zhang, S., Wu, H., 2007. Carbon isotope variability across the Ediacaran Yangtze platform in South China: Implications for a large surface-to-deep ocean <math>< i > 8 < /i > < sup > 13 < /sup > C gradient. *Earth*

- Planet. Sci. Lett. 261 (1), 303–320.
- Johnston, D.T., Macdonald, F.A., Gill, B.C., Hoffman, P.F., Schrag, D.P., 2012. Uncovering the Neoproterozoic carbon cycle. *Nature* 483, 320–323.
- Jones, D.S., Brothers, R.W., Crüger Ahm, A.-S., Slater, N., Higgins, J.A., Fike, D.A., 2020. Sea level, carbonate mineralogy, and early diagenesis controlled $\delta^{13}\text{C}$ records in Upper Ordovician carbonates. *Geology* 48 (2), 194–199.
- Kaufman, A.J., Hayes, J.M., Knoll, A.H., Germs, G.J.B., 1991. Isotopic compositions of carbonates and organic carbon from upper Proterozoic successions in Namibia: stratigraphic variation and the effects of diagenesis and metamorphism. *Precambr. Res.* 49 (3), 301–327.
- Kaufman, A., Knoll, A., 1995. Neoproterozoic variations in the C-isotopic composition of seawater: stratigraphic and biogeochemical implications. *Precambr. Res.* 73 (1–4), 27–49.
- Khain, E.V., Bibikova, E.V., Salnikova, E.B., Kroener, A., Gibsher, A.S., Didenko, A.N., Degtyarev, K.E., Fedotova, A.A., 2003. The palaeo-Asian ocean in the Neoproterozoic and early Palaeozoic: New geochronologic data and palaeotectonic reconstructions. *Precambr. Res.* 122, 329–358.
- Lacazette, A., 1990. Application of linear elastic fracture mechanics to the quantitative evaluation of fluid-inclusion decrepitation. *Geology* 18 (8), 782–785.
- Land, L.S., 1985. The origin of massive dolomite. *J. Geol. Educ.* 33 (2), 112–125.
- Lavoie, D., Chi, G., 2010. Lower Paleozoic foreland basins in eastern Canada: tectono-thermal events recorded by faults, fluids and hydrothermal dolomites. *Bull. Can. Pet. Geol.* 58 (1), 17–35.
- Lexa, O., Tomurhuu, D., 2010. Early Cambrian eclogites in SW Mongolia: evidence that the Palaeo-Asian Ocean suture extends further east than expected. *J. Metamorph. Geol.* 28, 915–933.
- Lucia, F.J., 1995. Rock-fabric/petrophysical classification of carbonate pore space for reservoir characterization. *AAPG Bull.* 79 (9), 1275–1300.
- Luczaj, J.A., 2006. Evidence against the Dorag (mixing-zone) model for dolomitization along the Wisconsin archA case for hydrothermal diagenesis. *Bulletin* 90 (11), 1719–1738.
- Lugli, S., Torres-Ruiz, J., Garuti, G., Olmedo, F., 2000. Petrography and geochemistry of the Euguí magnesite deposit (Western Pyrenees, Spain): evidence for the development of a peculiar zebra banding by dolomite replacement. *Econ. Geol.* 95 (8), 1775–1791.
- Macdonald, F.A., Jones, D.S., Schrag, D.P., 2009a. Stratigraphic and tectonic implications of a new glacial diamictite-cap carbonate couplet in southwestern Mongolia. *Geology* 37, 123–126.
- Macdonald, F.A., McClelland, W.C., Schrag, D.P., Macdonald, W.P., 2009b. Neoproterozoic glaciation on a carbonate platform margin in Arctic Alaska and the origin of the North Slope subterrane. *Geol. Soc. Am. Bull.* 121 (3–4), 448–473.
- Macdonald, F.A., Schmitz, M.D., Strauss, J.V., Halverson, G.P., Gibson, T.M., Eyster, A., Cox, G., Mamrol, P., Crowley, J.L., 2018. Cryogenian of Yukon. *Precambr. Res.* 319, 114–143.
- Melchin, M.J., Holmden, C., 2006. Carbon isotope chemostratigraphy of the Llandovery in Arctic Canada: implications for global correlation and sea-level change. *Geol. Foeren. Stockholm Foerh.* 128 (2), 173–180.
- Morrow, D.W., 1982. Diogenesis 1. Dolomite-Part 1: The chemistry of dolomitization and dolomite precipitation. *Geosci. Can.* 9, no. 1.
- Nogues, J.P., Fitts, J.P., Celia, M.A., Peters, C.A., 2013. Permeability evolution due to dissolution and precipitation of carbonates using reactive transport modeling in pore networks: Permeability evolution due to reaction of carbonates. *Water Resour. Res.* 49 (9), 6006–6021.
- Oehlert, A.M., Swart, P.K., 2014. Interpreting carbonate and organic carbon isotope covariance in the sedimentary record. *Nat. Commun.* 5, 4672.
- Osborne, M., Haszeldine, S., 1993. Evidence for resetting of fluid inclusion temperatures from quartz cements in oilfields. *Mar. Pet. Geol.* 10 (3), 271–278.
- Polito, P.A., Kyser, T.K., Golding, S.D., Southgate, P.N., 2006. Zinc deposits and related mineralization of the Burkettown Mineral Field, including the World-Class Century Deposit, Northern Australia: fluid inclusion and stable isotope evidence for basin fluid sources. *Econ. Geol.* 101 (6), 1251–1273.
- Radke, B.M., Mathis, R.L., 1980. On the formation and occurrence of saddle dolomite. *J. Sediment. Res.* 50 (4).
- Rooney, A.D., Strauss, J.V., Brandon, A.D., Macdonald, F.A., 2015. A Cryogenian chronology: Two long-lasting synchronous Neoproterozoic glaciations. *Geology* 43 (5), 459–462. <https://doi.org/10.1130/G36511.1>.
- Rose, C.V., Swanson-Hysell, N.L., Husson, J.M., Poppick, L.N., Cottle, J.M., Schoene, B., Maloof, A.C., 2012. Constraints on the origin and relative timing of the Trezona $\delta^{13}\text{C}$ anomaly below the end-Cryogenian glaciation. *Earth Planet. Sci. Lett.* 319, 241–250.
- Saltzman, M.R., Sedlacek, A.R., 2013. Chemostratigraphy indicates a relatively complete Late Permian to Early Triassic sequence in the western United States. *Geology* 41 (4), 399–402.
- Saltzman, M.R., Thomas, E., 2012. Carbon Isotope Stratigraphy, The Geologic Time Scale. Elsevier, pp. 207–232.
- Sander, B., 1951. Contributions to the Study of Depositional Fabrics. American Association of Petroleum Geologists.
- Smith, E.F., Macdonald, F.A., Petach, T.A., Bold, U., Schrag, D.P., 2016. Integrated stratigraphic, geochemical, and paleontological late Ediacaran to early Cambrian records from southwestern Mongolia. *Geol. Soc. Am. Bull.* 128, 442–468.
- Swart, P.K., 2008. Global synchronous changes in the carbon isotopic composition of carbonate sediments unrelated to changes in the global carbon cycle. *Proc. Natl. Acad. Sci.* 105 (37), 13741–13745.
- Swart, P.K., Eberli, G.P., 2005. The nature of $\delta^{13}\text{C}$ of periplatform sediments: implications for stratigraphy and the global carbon cycle. *Sed. Geol.* 175, 115–129.
- Swennen, R., Vandeginste, V., Ellam, R., 2003. Genesis of zebra dolomites (Cathedral Formation: Canadian Cordillera Fold and Thrust Belt, British Columbia). *J. Geochem. Explor.* 78–79, 571–577.
- Tamer, A., 1965. Chemical staining methods used in the identification of carbonate minerals.
- Vandeginste, V., Sweenen, R., Gleeson, S.A., Ellam, R.M., Osadetz, K., Roure, F., 2005. Zebra dolomitization as a result of focused fluid flow in the Rocky Mountains Fold and Thrust Belt, Canada. *Sedimentology* 52, 1067–1095.
- Veizer, J., Ala, D., Azmy, K., Bruckschen, P., Buhl, D., Bruhn, F., Carden, G.A.F., Diener, A., Ebnet, S., Godderis, Y., Jasper, T., Korte, C., Pawelleck, F., Podlaha, O.G., Stauss, H., 1999. $^{87}\text{Sr}/^{86}\text{Sr}$, $\delta^{13}\text{C}$ and $\delta^{18}\text{O}$ evolution of Phanerozoic seawater. *Chem. Geol.* 161, 59–88.
- Warren, J., 2000. Dolomite: occurrence, evolution and economically important associations. *Earth Sci. Rev.* 52 (1), 1–81.
- Wiegand, B. A., Brehme, M., Kamah, Y., and Sauter, M., 2015, Distribution of Sr and Ca Isotopes in Fluids of Lahendong Geothermal Field: Proceedings World Geothermal Congress 2015.
- Windley, B.F., Alexeiev, D., Xiao, W., Kröner, A., Badarch, G., 2007. Tectonic models for accretion of the Central Asian Orogenic Belt. *J. Geol. Soc.* 164 (1), 31–47.
- Yang, J., Jansen, M.F., Macdonald, F.A., Abbot, D.S., 2017. Persistence of a freshwater surface ocean after a snowball Earth. *Geology* 45 (7), 615–618.